NASA TECHNICAL MEMORANDUM

NASA TM X-2286

NASA TM X-2286

VERTICAL-FIN LOADS AND RUDDER HINGE-MOMENT MEASUREMENTS ON A 1/8-SCALE MODEL OF THE M2-F3 LIFTING BODY VEHICLE AT MACH NUMBERS FROM 0.50 TO 1.30

by Ming H. Tang

Flight Research Center
Edwards, Calif. 93523

NATIONAL AERONAUTICS AND SPACE ADMINISTRATION • WASHINGTON, D. C. • MAY 1971

1. Report No. NASA TM X-2286	2. Government Accession No.	3. Recipient's Catalog No.
4. Title and Subtitle VERTICAL-FIN LOADS AND RUDDER HINGE-MOMENT MEASUREMENTS ON A 1/8-SCALE MODEL OF THE M2-F3 LIFTING BODY VEHICLE AT MACH NUMBERS FROM 0.50 TO 1.30		5. Report Date May 1971 6. Performing Organization Code
7. Author(s) Ming H. Tang		8. Performing Organization Report No. H-650 10. Work Unit No. 727-00-00-01-24
9. Performing Organization Name and Address NASA Flight Research Center P. O. Box 273 Edwards, California 93523		11. Contract or Grant No. 13. Type of Report and Period Covered Technical Memorandum
12. Sponsoring Agency Name and Address National Aeronautics and Space Administration Washington, D. C. 20546		14. Sponsoring Agency Code

15. Supplementary Notes

16. Abstract

Outboard-fin loads and rudder hinge-moment measurements were obtained from a 1/8-scale model of the M2-F3 lifting body vehicle tested in the Ames Research Center's 11-Foot Transonic Wind Tunnel. The tests were conducted at Mach 0.50 to 1.30. The effects of variations in rudder deflection, upper-flap deflection, lower-flap deflection, and angles of attack and sideslip were studied.

The left-outboard-fin loads increased with increase in angle of attack, Mach number, rudder deflection, lower-flap deflection, and negative sideslip and decreased with increasing upper-flap deflection. The rudder hinge moment increased with increase in rudder deflection and, generally, with Mach number.

17. Key Words (Suggested by Author(s))	18. Distribution Statement
Lifting body vehicle - Aerodynamic loads	Unclassified - Unlimited

19. Security Classif. (of this report)	20. Security Classif. (of this page)	21. No. of Pages	22. Price*
Unclassified	Unclassified	42	$3.00

*For sale by the National Technical Information Service, Springfield, Virginia 22151

VERTICAL-FIN LOADS AND RUDDER HINGE-MOMENT MEASUREMENTS ON A 1/8-SCALE MODEL OF THE M2-F3 LIFTING BODY VEHICLE AT MACH NUMBERS FROM 0.50 TO 1.30

Ming H. Tang
Flight Research Center

INTRODUCTION

The development of maneuverable vehicles capable of controlled reentry from earth orbit to a tangential landing led to the development of three lifting body configurations, designated the M2-F2, HL-10, and X-24A. Flight vehicles using the three different configurations are being flight tested at the NASA Flight Research Center (refs. 1 and 2).

One of the three lifting body vehicles, the M2-F2, experienced handling-qualities problems during the flight-test program. Hence, when the vehicle was being repaired after a landing accident, various modifications were incorporated; the most notable was the addition of a center vertical fin. The rebuilt vehicle was redesignated the M2-F3 and returned to flight-test status.

In support of the M2-F3 flight-test program a 1/8-scale model of the vehicle was tested in the Ames Research Center's 11-Foot Transonic Wind Tunnel. As part of the overall aerodynamic loads investigation (refs. 3 and 4), outboard vertical-fin loads and rudder hinge moments were measured during the wind-tunnel tests.

The purpose of the wind-tunnel loads investigation was to provide aerodynamic loads data for use in establishing the structural envelope for the M2-F3 flight-test program and to provide wind-tunnel loads data for correlation with flight-test loads measurements in order to assess the reliability of using small-scale wind-tunnel tests in structural design. The results of this investigation are presented in this report.

SYMBOLS

Physical quantities are given in the International System of Units (SI) and parenthetically in U. S. Customary Units. The measurements were taken in U. S. Customary Units. Factors relating the two systems are presented in reference 5.

Sign conventions used for the parameters pertinent to this report are shown in figure 1.

b	outboard-fin reference span, 0.103 m (4.07 in.)
C_h	rudder hinge-moment coefficient, $\frac{H}{qS_r c_r}$
C_y	outboard-fin normal-force coefficient, $\frac{N}{qS}$
c_i	outboard-fin local chord, i = 0, 1, 2, 3, m (in.)
c_r	rudder chord, 0.048 m (1.87 in.)
$\bar{c}$	outboard-fin reference mean aerodynamic chord, 0.202 m (7.97 in.), located 0.055 m (2.15 in.) up from the horizontal reference line
H	rudder hinge moment, m-N (in-lb)
M	free-stream Mach number
N	fin normal force, N (lb)
q	free-stream dynamic pressure, N/m^2 ($lb/in.^2$ or lb/ft^2)
S	outboard-fin reference area, 0.020 m^2 (30.59 $in.^2$)
S_r	rudder reference area, 0.008 m^2 (11.87 $in.^2$)
X, Y, Z	vehicle reference axes
x_{cp}	outboard-fin chordwise center-of-pressure location, measured from the leading edge of the reference mean aerodynamic chord, fraction of $\bar{c}$
z_{cp}	outboard-fin spanwise center-of-pressure location, measured from the horizontal reference line, fraction of b
α	angle of attack, deg

β angle of sideslip, deg

δ control-surface deflection, deg

Subscripts:

l lower flap

r rudder

u upper flap

APPARATUS AND MODEL

Wind Tunnel

The investigation was made in the Ames 11-Foot Transonic Wind Tunnel (Unitary), a closed-return, variable-density tunnel with a 3.35-meter-square (11-foot-square) test section. The tunnel has an adjustable nozzle with two flexible walls and a slotted test section to permit transonic testing up to Mach 1.4. The total pressure of the tunnel air can be varied from a minimum value of 0.0506 MN/m^2 (0.5 atmosphere) to a maximum of 0.2279 MN/m^2 (2.25 atmosphere). The stagnation temperature is 580° R (322° K).

Model

The 1/8-scale M2-F3 model mounted in the 11-Foot Transonic Wind Tunnel is shown in figures 2(a) and 2(b). The M2-F3 vehicle is basically half of a 26° cone with a rounded nose, faired afterbody, two outboard vertical fins, a center vertical fin, and five control surfaces. A three-view drawing of the model is shown in figure 3.

The left outboard fin and rudder on the model were instrumented with pressure orifices for fin load and rudder hinge-moment measurements. The locations of the 38 pressure orifices used are shown in figure 4.

TESTS, DATA REDUCTION, AND ACCURACY

Tests

The investigation was made at Mach numbers from 0.50 to 1.30, at dynamic pressures from 19,920 N/m^2 (416 lb/ft^2) to 39,500 N/m^2 (825 lb/ft^2), and at Reynolds

numbers of approximately 11.1×10^6, based on the model reference length of 0.846 meter (2.775 feet). The angle of attack was varied from approximately -10° to 21°. The various control-surface deflections were obtained by attaching angled brackets between the control surfaces and the model.

The investigation included tests to determine the fin normal-force coefficient and center-of-pressure variation due to changes in angle of attack, rudder position, upper-flap position, lower-flap position, angle of sideslip, and Mach number. Variation of rudder hinge-moment coefficient due to changes in angle of attack, rudder position, and Mach number was also investigated.

Data Reduction

The outboard-fin load coefficient and center of pressure and the rudder hinge-moment coefficient were obtained from model pressure data.

The net pressure coefficients were integrated chordwise along three span stations (fig. 4) and then integrated again spanwise to obtain the normal-force coefficient. The torque and the bending-moment coefficients were obtained in a similar manner and then converted to center-of-pressure locations; x_{cp} is in terms of percent of the mean aerodynamic chord from the leading edge of $\bar{c}$, and z_{cp} is in terms of percent of the reference span, b, from the horizontal reference line.

The rudder hinge moment was calculated by assuming a constant pressure distribution for the area assigned to each orifice. The sum of the products of the individual net pressures and the respective reference dimensions was then normalized with respect to the product of the rudder area and rudder chord.

Accuracy

The accuracy of the measured quantities presented, based on calibrations and repeatability of data, is estimated to be within the following limits:

C_y	±0.01
C_h	±0.01
x_{cp}	±0.01
z_{cp}	±0.01
α, deg	±0.02
β, deg	±0.02
M	±0.01

RESULTS AND DISCUSSION

The loads results from the wind-tunnel tests of the 1/8-scale M2-F3 model are

presented in figures 5 to 11. The test conditions associated with these results are presented in table 1.

Outboard-Fin Loads and Center-of-Pressure Locations

The left-outboard-fin normal-force coefficient and center of pressure are plotted against angle of attack in figures 5 to 8 and against Mach number in figure 9. In general, the outboard-fin normal-force coefficient increases with increasing angle of attack until apparent flow separation occurs, from which point the normal-force coefficient decreases with increasing angle of attack. The point of apparent flow separation occurs at a lower angle of attack with increasing Mach number.

Figure 5 shows the outboard-fin normal-force coefficient and chordwise center-of-pressure increase with increasing rudder deflection at Mach 0.50 to 1.30. The C_y variation due to rudder deflection is larger at low angles of attack and decreases with increasing angle of attack at transonic Mach numbers. The x_{cp} variation due to rudder deflection also decreases with increasing angle of attack at Mach 0.50 to 1.10. The spanwise center of pressure, z_{cp}, shows no change with rudder deflection.

Figure 6 indicates that C_y decreases with increasing upper-flap deflections at Mach 0.50 to 0.95. At Mach 1.10 and 1.30 the upper flaps have virtually no effect on the outboard-fin loads at high angle of attack. The value of x_{cp} also decreases with increasing upper-flap deflection. Transonically, this effect is more pronounced at low angles of attack. Figure 6 also indicates a very small increase in z_{cp} due to increase in upper-flap deflections at the low angles of attack.

Figure 7 shows that C_y increases with increasing lower-flap deflections at Mach 0.80, 0.90, and 0.95 (data were not available at Mach 0.50 and 0.70) and increases only slightly for high angles of attack at Mach 1.10 and 1.30. In general, both x_{cp} and z_{cp} show no variation due to changes in lower-flap positions; however, at Mach 0.95, x_{cp} increases with increasing lower-flap deflections.

Figure 8 indicates that C_y increases with negative sideslip and the effect of sideslip on the outboard-fin load is more pronounced at low angles of attack. In general, z_{cp} was not affected by variation in angle of sideslip.

Figure 9 shows typical variations of C_y, x_{cp}, and z_{cp} due to changes in Mach number. In general, C_y increases slightly from Mach 0.50 to 0.80. Between Mach 0.80 and 1.10, C_y increases more rapidly with Mach number, and then remains constant from Mach 1.10 to 1.30. From Mach 0.50 to 0.80, x_{cp} decreases and then increases from Mach 0.80 to 1.30; z_{cp} remains virtually constant throughout the Mach range.

Rudder Hinge Moments

The left-rudder hinge-moment coefficient is plotted against angle of attack in figure 10 and against Mach number in figure 11.

Figure 10 indicates that C_h increases with increasing rudder deflection throughout the Mach range investigated. The variation of C_h due to rudder position becomes less linear from Mach 0.95 to 1.30. The variation of C_h due to angle of attack is relatively small.

The rudder hinge-moment coefficient, C_h, shows the same trend with changes in Mach number as the normal-force coefficient, C_y. Figure 11 indicates that C_h increases slightly between Mach 0.50 and 0.80, increases more rapidly between Mach 0.80 to 1.10, and remains constant from Mach 1.10 to 1.30.

CONCLUSIONS

Vertical-fin loads and rudder hinge-moment measurements were obtained from wind-tunnel tests on a 1/8-scale model of the M2-F3 lifting body. Results from the tests showed that:

1. The left-outboard-fin normal-force coefficient increased with increase in angle of attack (until the point of apparent flow separation), Mach number, rudder deflection, lower-flap deflection, and negative sideslip, and decreased with increasing upper-flap deflection.

2. The left-outboard-fin chordwise center of pressure in general increased with increase in rudder deflection, decreased with increasing upper-flap deflection, and indicated an increase transonically.

3. The left-outboard-fin spanwise center of pressure in general was not affected by variations in control-surface deflection, angle of sideslip, or Mach number.

4. The left-rudder hinge-moment coefficient increased with increase in rudder deflection, and, similar to the outboard-fin normal-force coefficient, increased slightly with change in Mach number between 0.50 and 0.80, increased more rapidly between 0.80 and 1.10, and remained constant from 1.10 to 1.30.

Flight Research Center,
National Aeronautics and Space Administration,
Edwards, Calif., January 8, 1971.

REFERENCES

1. Thompson, Milton O.; Peterson, Bruce A.; and Gentry, Jerauld R.: Lifting-Body Flight Test Program. SETP Technical Review, second 1966 issue, vol. 8, no. 2, Sept. 1966, pp. 1-22.

2. Tang, Ming H.: Correlation of Flight-Test Loads With Wind-Tunnel Predicted Loads on Three Lifting Body Vehicles. Flight-Test Results Pertaining to the Space Shuttlecraft, NASA TM X-2101, 1970, pp. 59-72.

3. Jenkins, Jerald M.; Tang, Ming H.; and Pearson, George, P. E.: Vertical-Tail Loads and Control-Surface Hinge-Moment Measurements on the M2-F2 Lifting Body During Initial Subsonic Flight Tests. NASA TM X-1712, 1968.

4. Tang, Ming H.; and DeAngelis, Michael V.: Fin Loads and Control-Surface Hinge Moments Measured in Full-Scale Wind-Tunnel Tests on the X-24A Flight Vehicle. NASA TM X-1922, 1969.

5. Mechtly, E. A.: The International System of Units - Physical Constants and Conversion Factors. NASA SP-7012, 1969.

TABLE 1. – TEST CONDITIONS

Coefficients presented	Figure number	M	α, deg	β, deg	δ_u, deg	δ_l, deg	δ_r, deg
C_y, x_{cp}, z_{cp}	5(a)	0.50	-10 to 20	0	-20	35	0, 10, 25
	5(b)	.70	-10 to 21	0	-20	35	0, 10, 25
	5(c)	.80	-10 to 21	0	-20	35	0, 5, 15, 25
	5(d)	.90	-10 to 21	0	-20	35	0, 5, 15, 25
	5(e)	.95	-10 to 21	0	-20	35	0, 5, 15, 25
	5(f)	1.10	-10 to 21	0	-20	35	0, 5, 15, 25
	5(g)	1.30	-10 to 21	0	-20	35	0, 5, 15, 25
C_y, x_{cp}, z_{cp}	6(a)	0.50	-10 to 20	0	-15, -20	35	0
	6(b)	.70	-10 to 21	0	-15, -20	35	0
	6(c)	.80	-10 to 21	0	-15, -20, -25	35	0
	6(d)	.90	-10 to 21	0	-15, -20, -25	35	0
	6(e)	.95	-10 to 21	0	-15, -20, -25	35	0
	6(f)	1.10	-10 to 21	0	-15, -20, -25	35	0
	6(g)	1.30	-10 to 21	0	-15, -20, -25	35	0
C_y, x_{cp}, z_{cp}	7(a)	0.80	-10 to 21	0	-20	25, 35, 45	0
	7(b)	.90	-10 to 21	0	-20	25, 35, 45	0
	7(c)	.95	-10 to 21	0	-20	25, 35, 45	0
	7(d)	1.10	-10 to 21	0	-20	25, 35, 45	0
	7(e)	1.30	-10 to 21	0	-20	25, 35, 45	0
C_y, x_{cp}, z_{cp}	8(a)	0.80	-10 to 21	-4, 0, 4	-20	35	0
	8(b)	.90	-10 to 21	-4, 0, 4	-20	35	0
	8(c)	.95	-10 to 21	-4, 0, 4	-20	35	0
	8(d)	1.10	-10 to 21	-4, 0, 4	-20	35	0
	8(e)	1.30	-10 to 21	-4, 0, 4	-20	35	0
C_y, x_{cp}, z_{cp}	9	0.50 to 1.30	0	0	-20	35	0
C_h	10(a)	0.50	-10 to 20	0	-20	35	10, 25
	10(b)	.70	-10 to 21	0	-20	35	10, 25
	10(c)	.80	-10 to 21	0	-20	35	0, 5, 10, 15, 25
	10(d)	.90	-10 to 21	0	-20	35	0, 5, 10, 15, 25
	10(e)	.95	-10 to 21	0	-20	35	0, 5, 10, 15, 25
	10(f)	1.10	-10 to 21	0	-20	35	0, 5, 10, 15, 25
	10(g)	1.30	-10 to 21	0	-20	35	0, 5, 10, 15, 25
C_h	11	0.50 to 1.30	0	0	-20	35	10

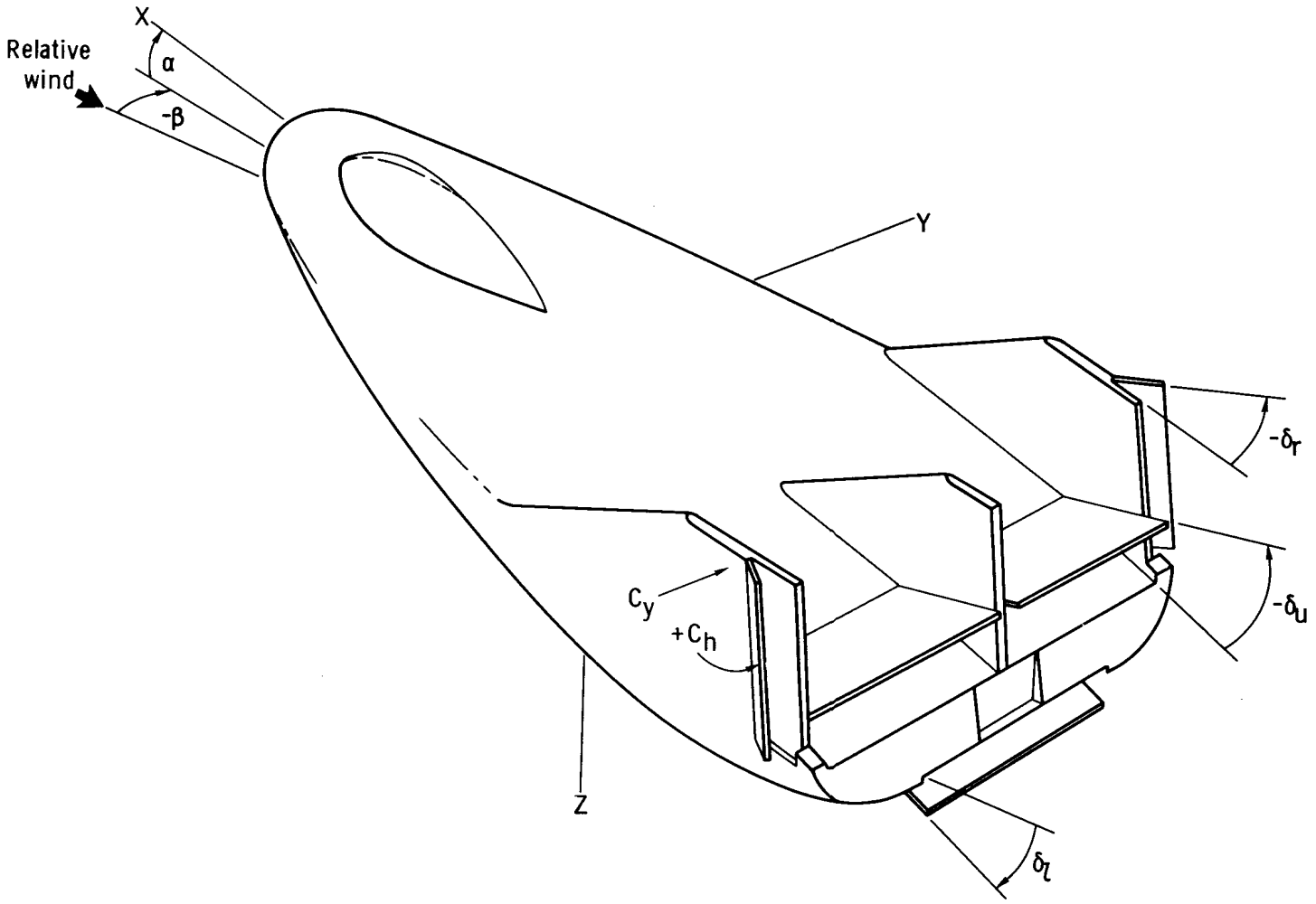

Figure 1. Sign convention for the M2-F3 vehicle.

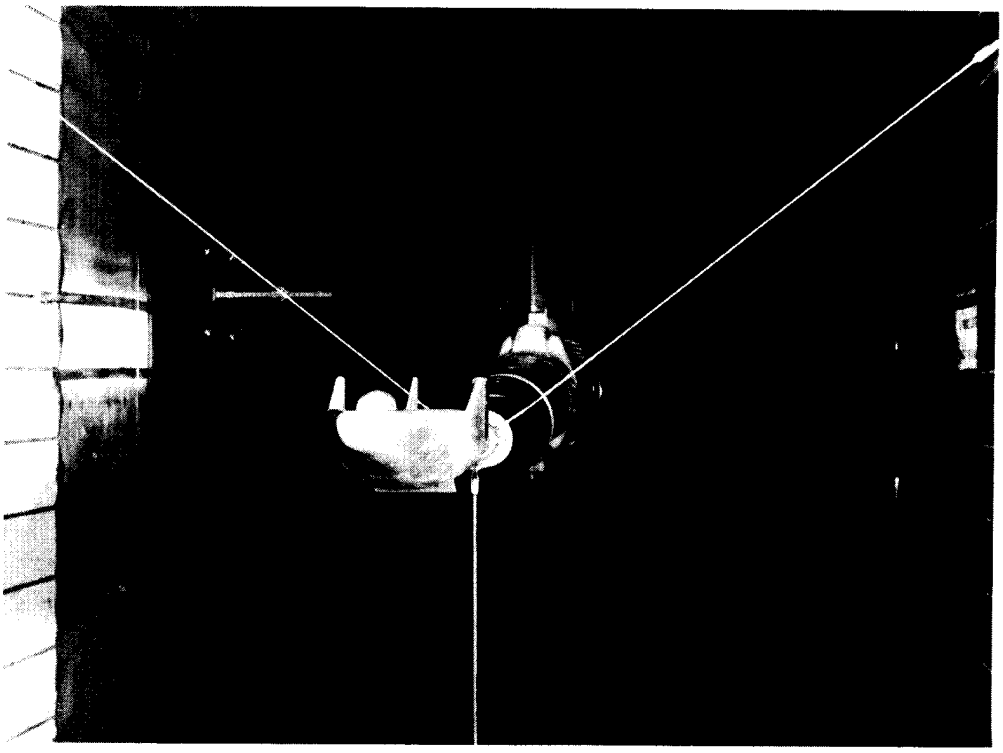

(a) Three-quarter front view.

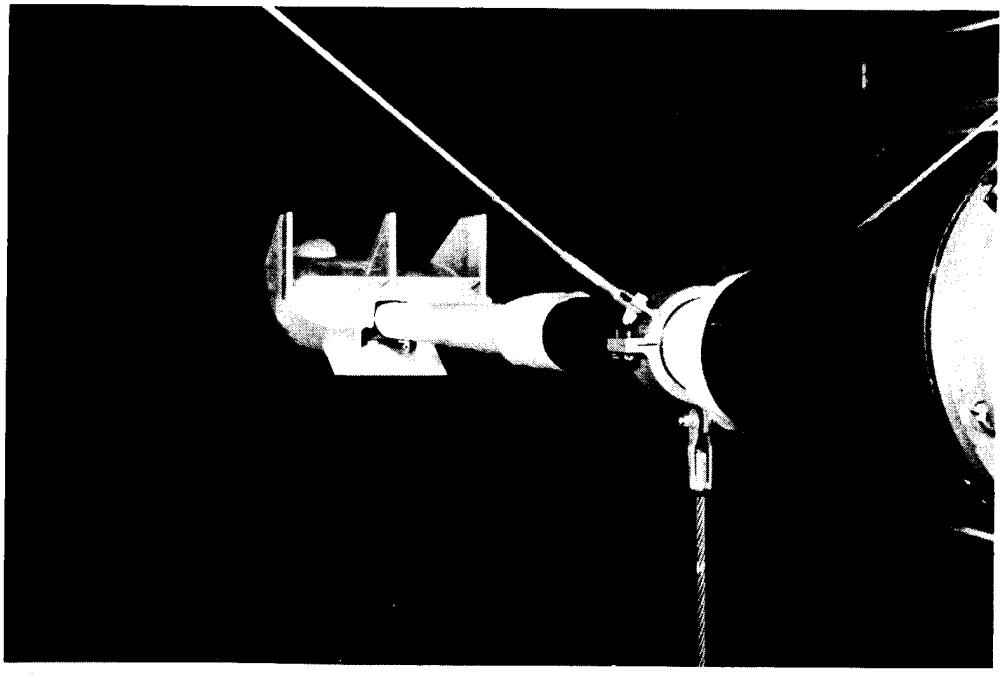

(b) Three-quarter rear view.

Figure 2. One-eighth-scale M2-F3 model mounted in the 11-Foot Transonic Wind Tunnel.

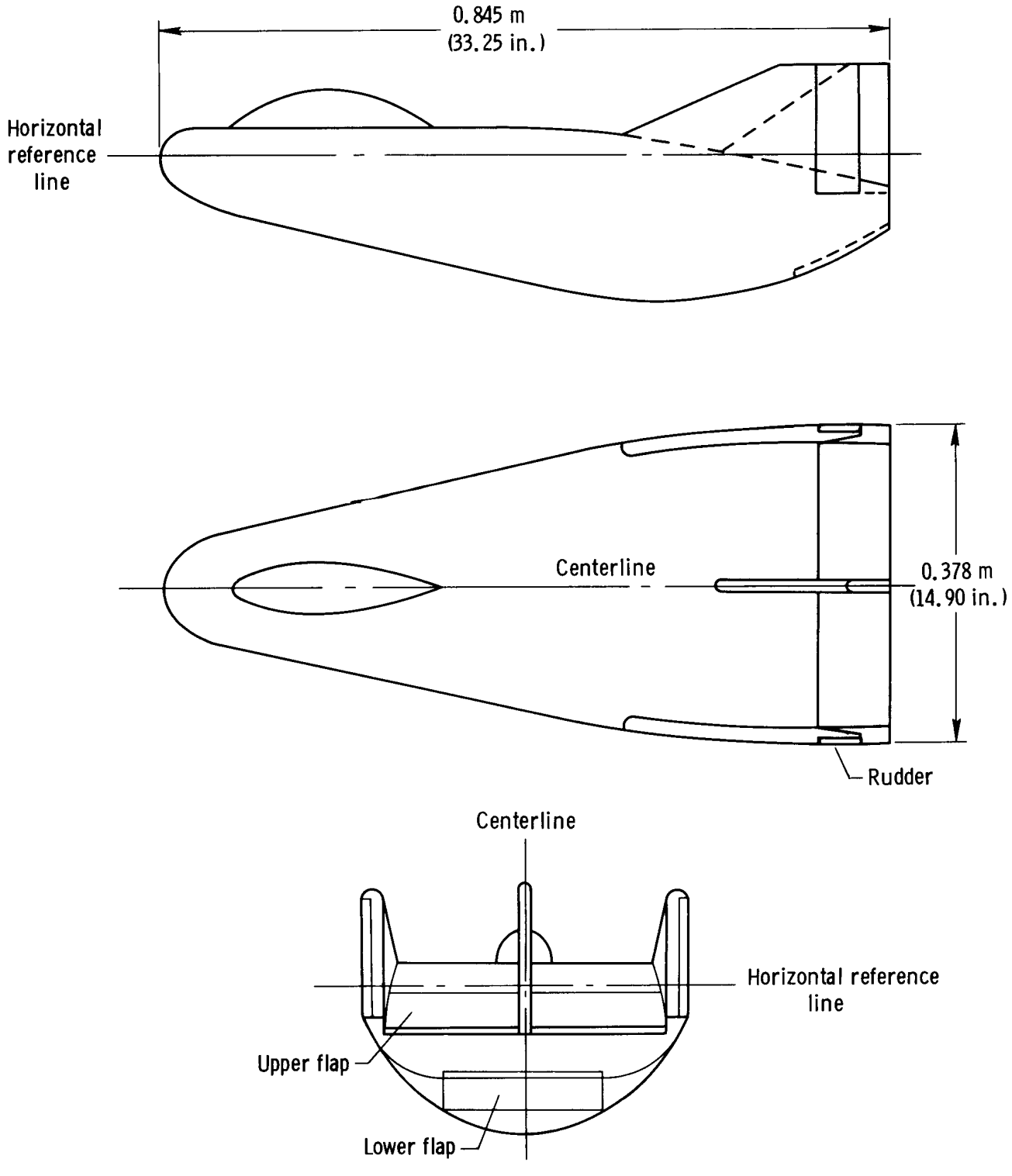

Figure 3. Three-view drawing of the M2-F3 model.

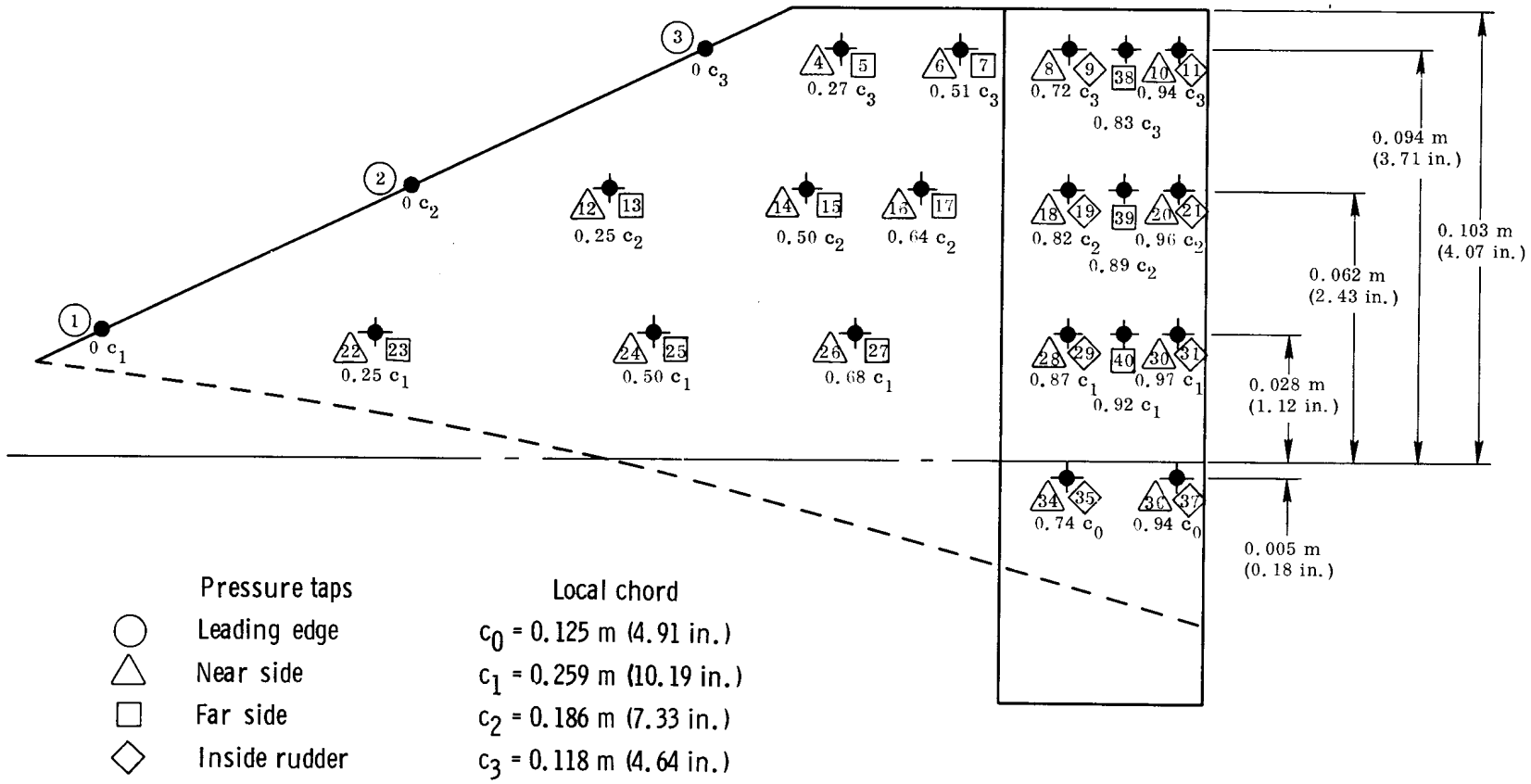

Figure 4. Pressure-orifice locations on the left-hand fin and rudder of the M2-F3 model.

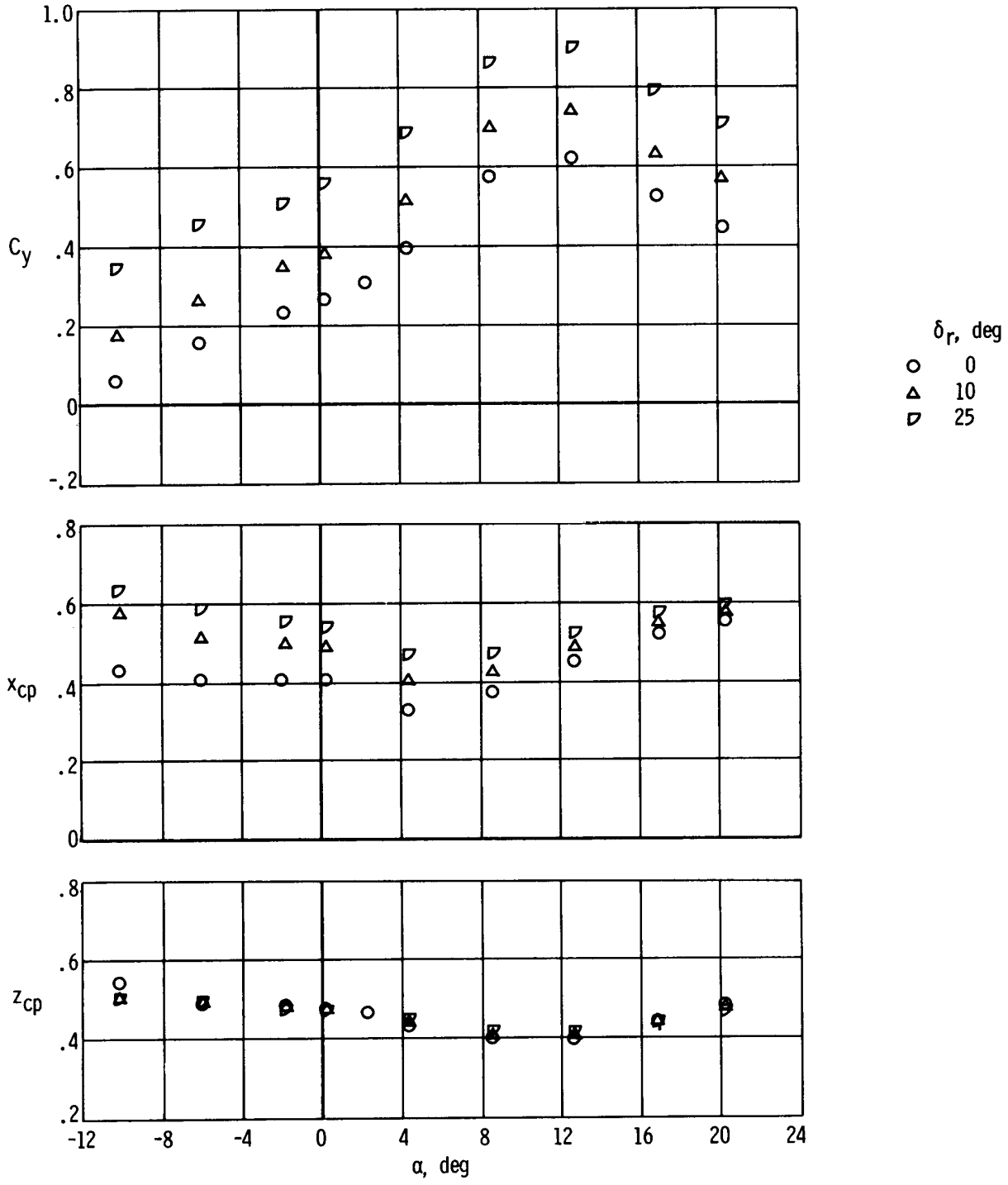

(a) M = 0.50.

Figure 5. Variation of the left-outboard-fin normal-force coefficient and center of pressure with angle of attack and rudder position. $\beta = 0°$; $\delta_u = -20°$; $\delta_l = 35°$.

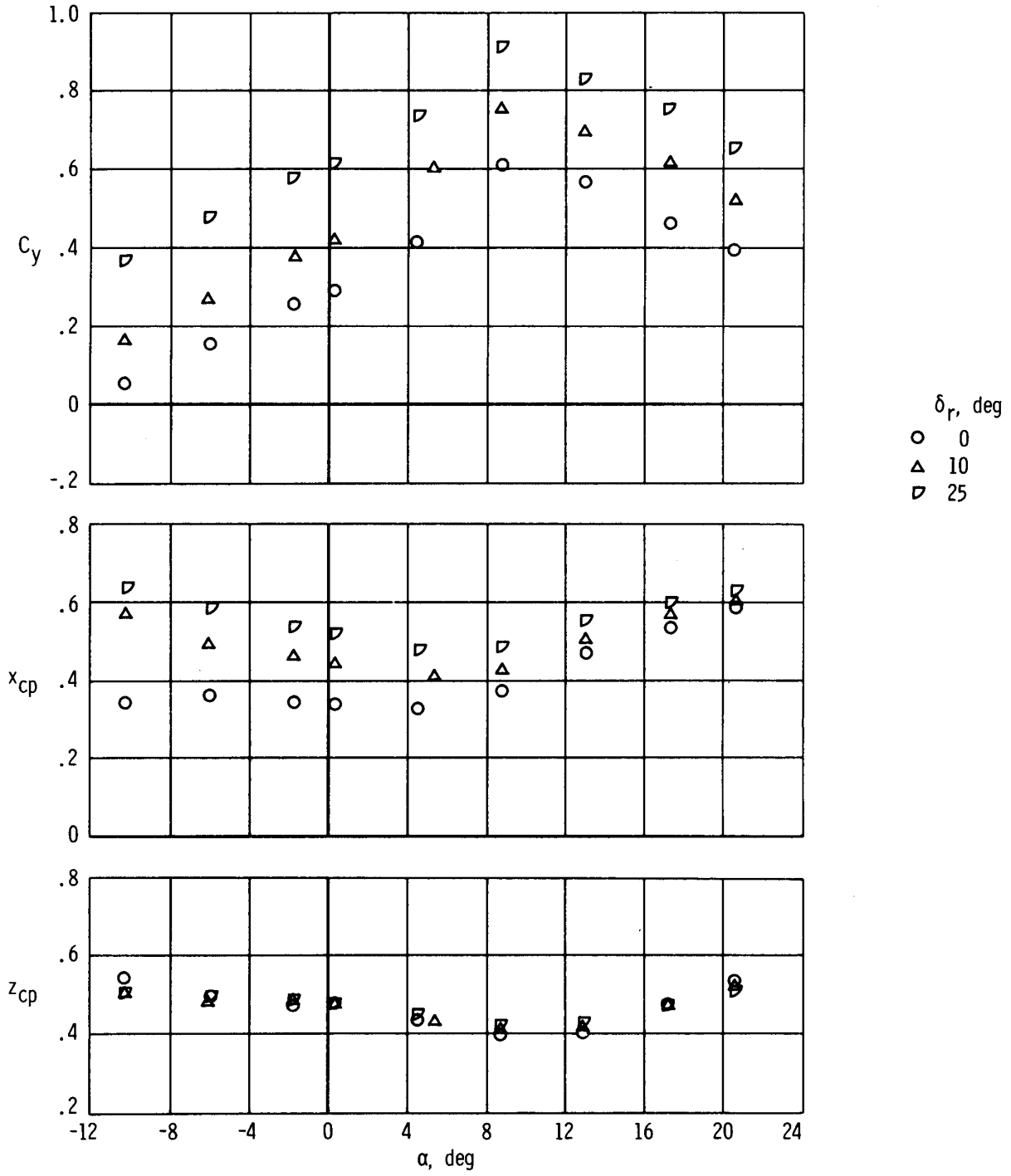

(b) M = 0.70.

Figure 5. Continued.

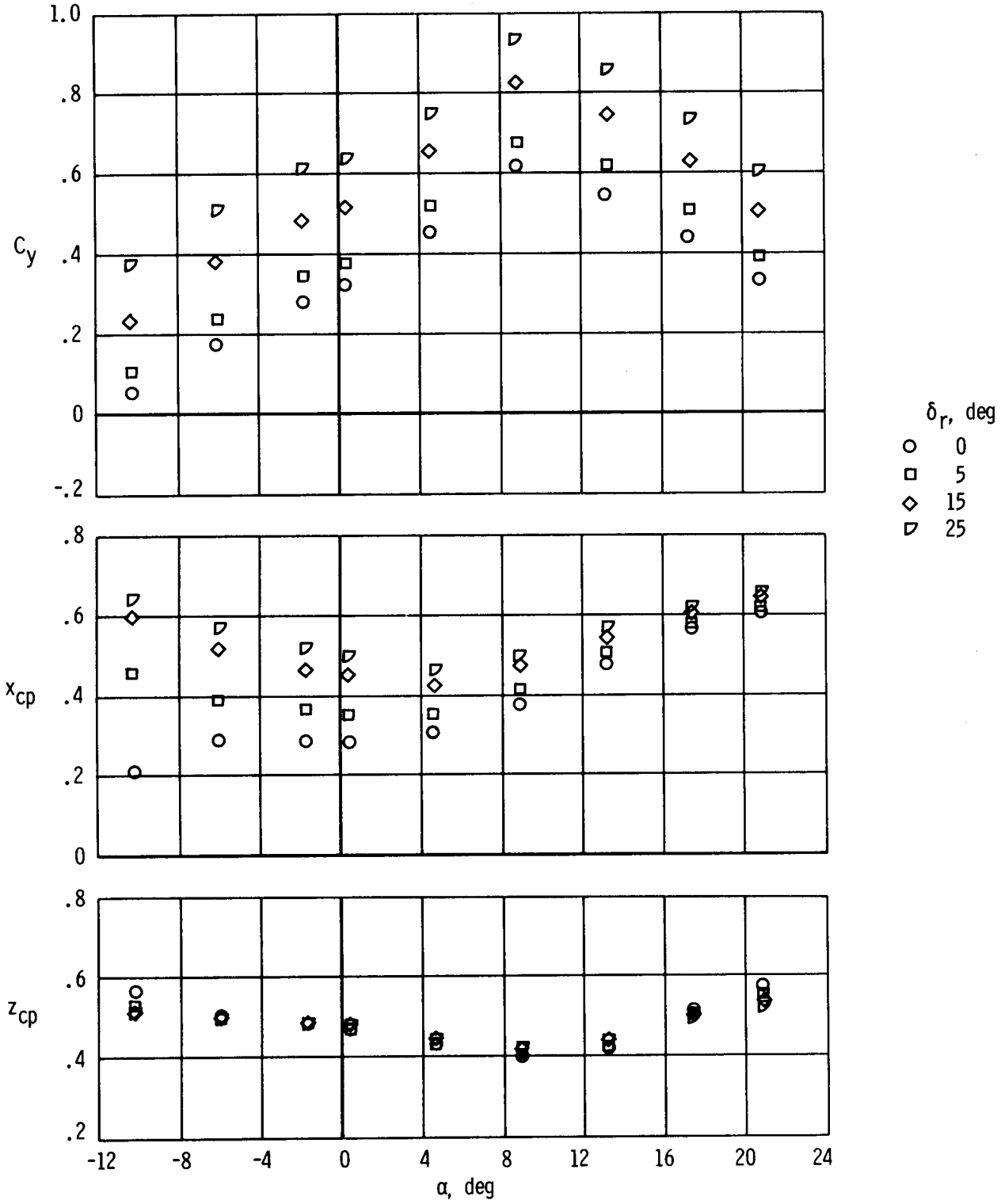

(c) M = 0.80.

Figure 5. Continued.

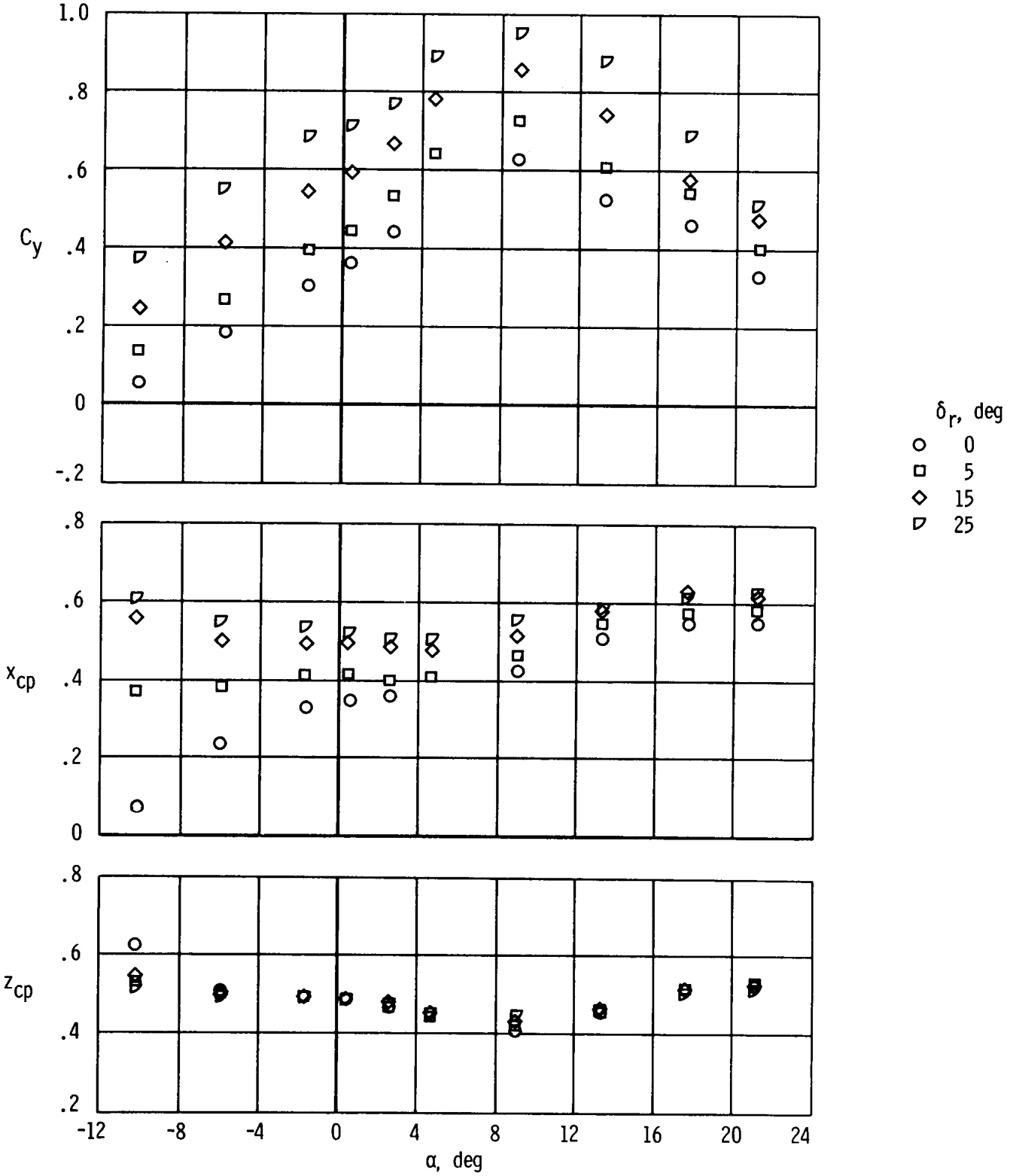

(d) M = 0.90.

Figure 5. Continued.

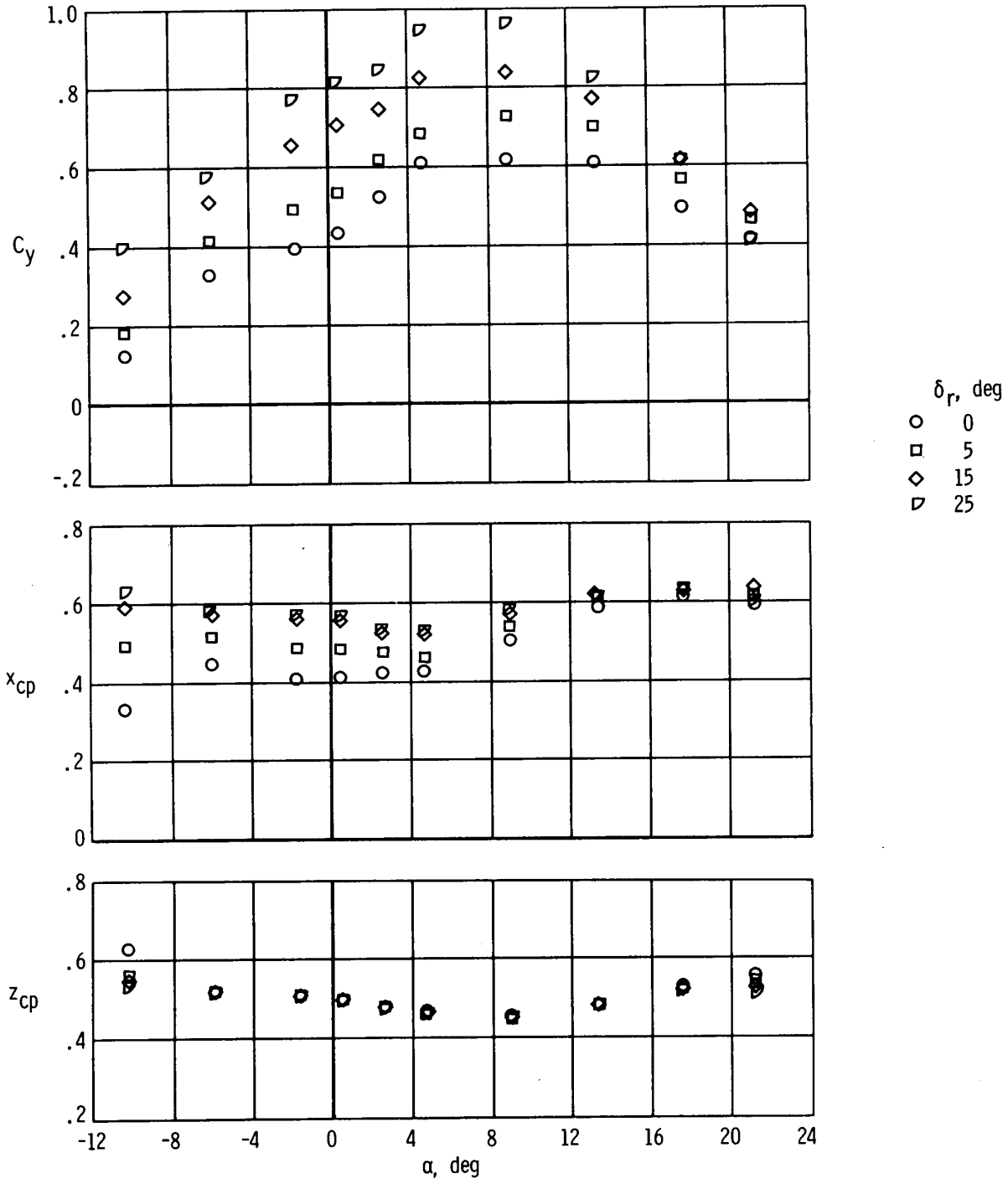

(e) M = 0.95.

Figure 5. Continued.

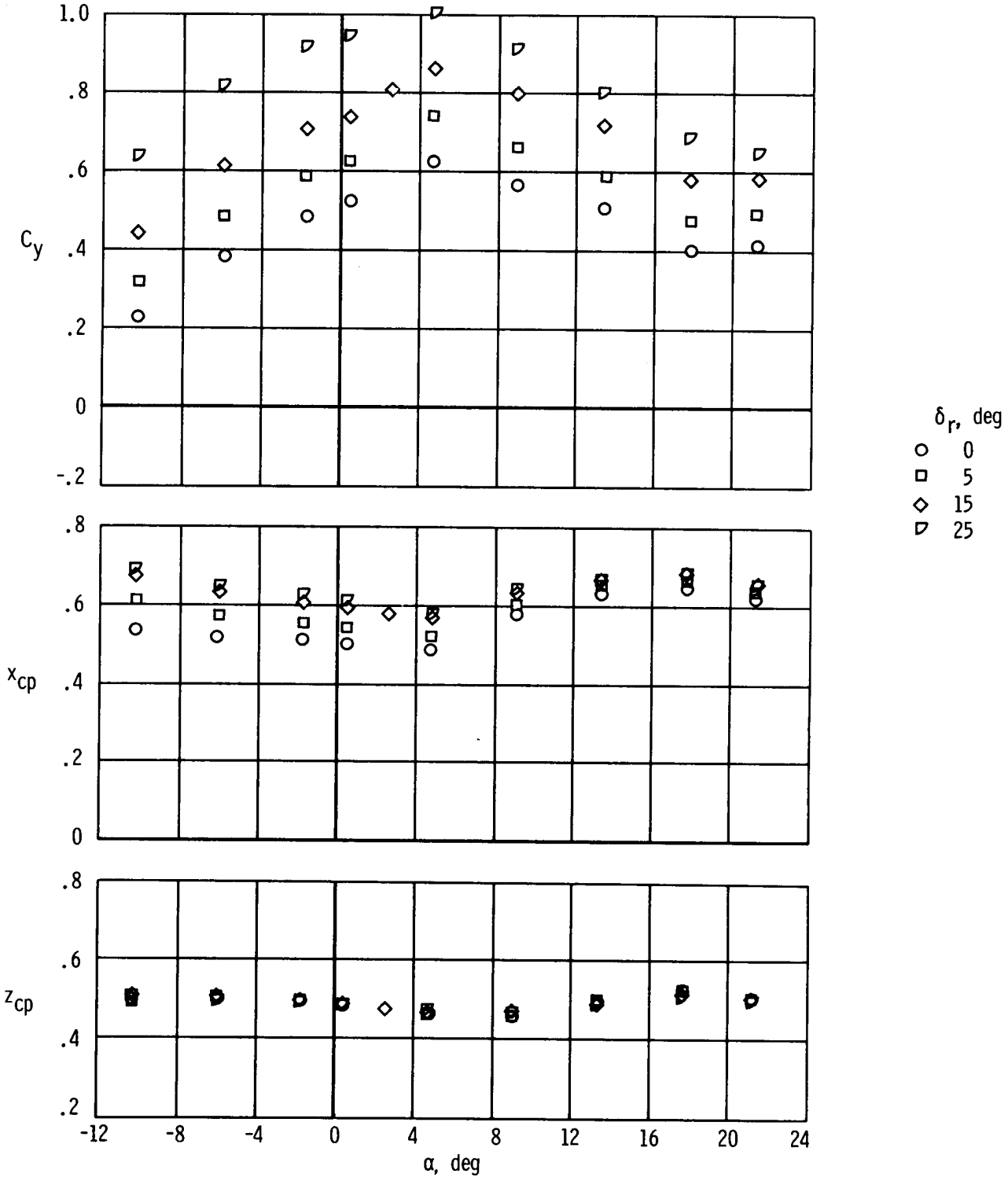

(f) M = 1.10.

Figure 5. Continued.

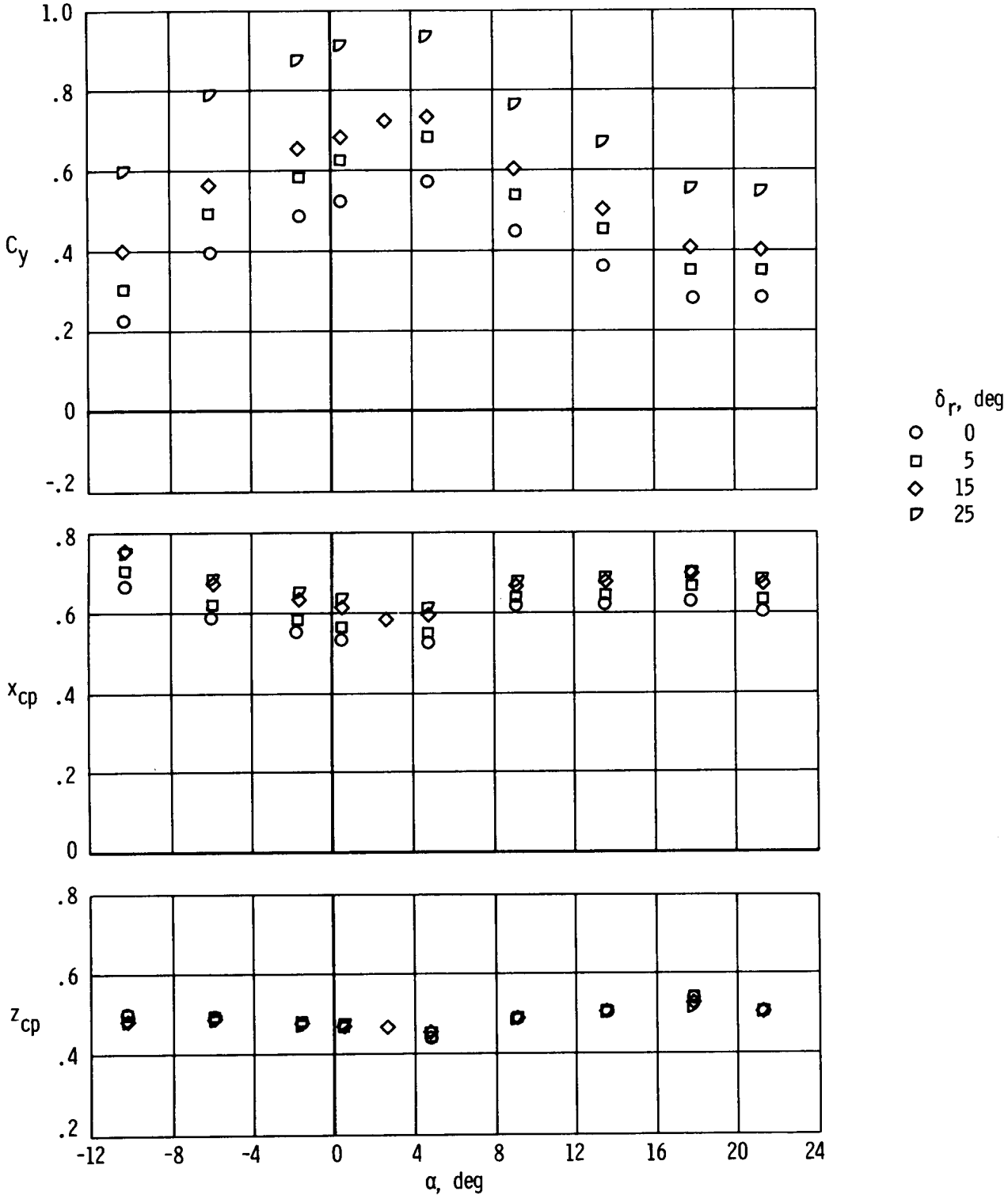

(g) M = 1.30.

Figure 5. Concluded.

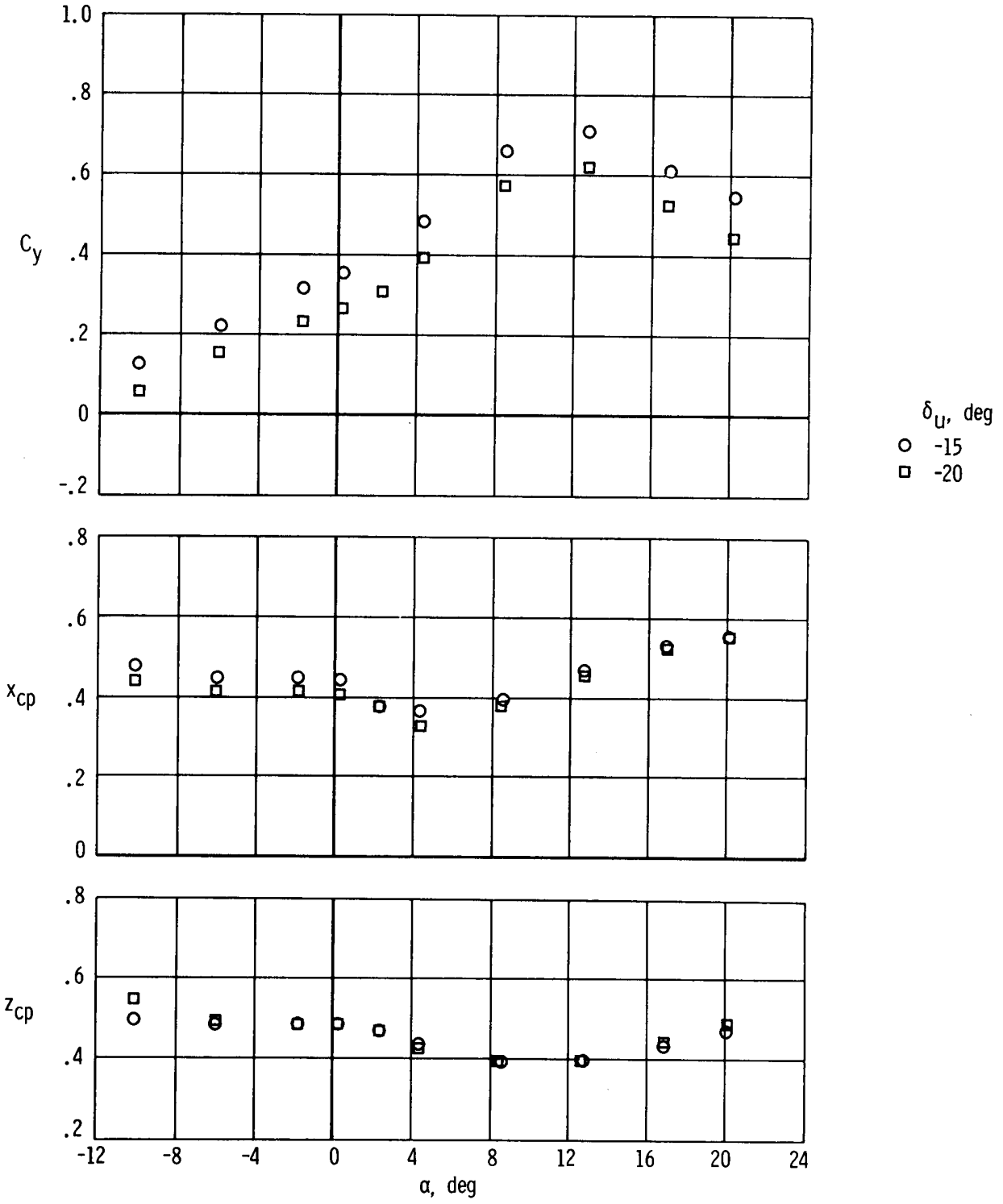

(a) M = 0.50.

Figure 6. Variation of the left-outboard-fin normal-force coefficient and center of pressure with angle of attack and upper-flap position. $\beta = 0°$; $\delta_r = 0°$; $\delta_l = 35°$.

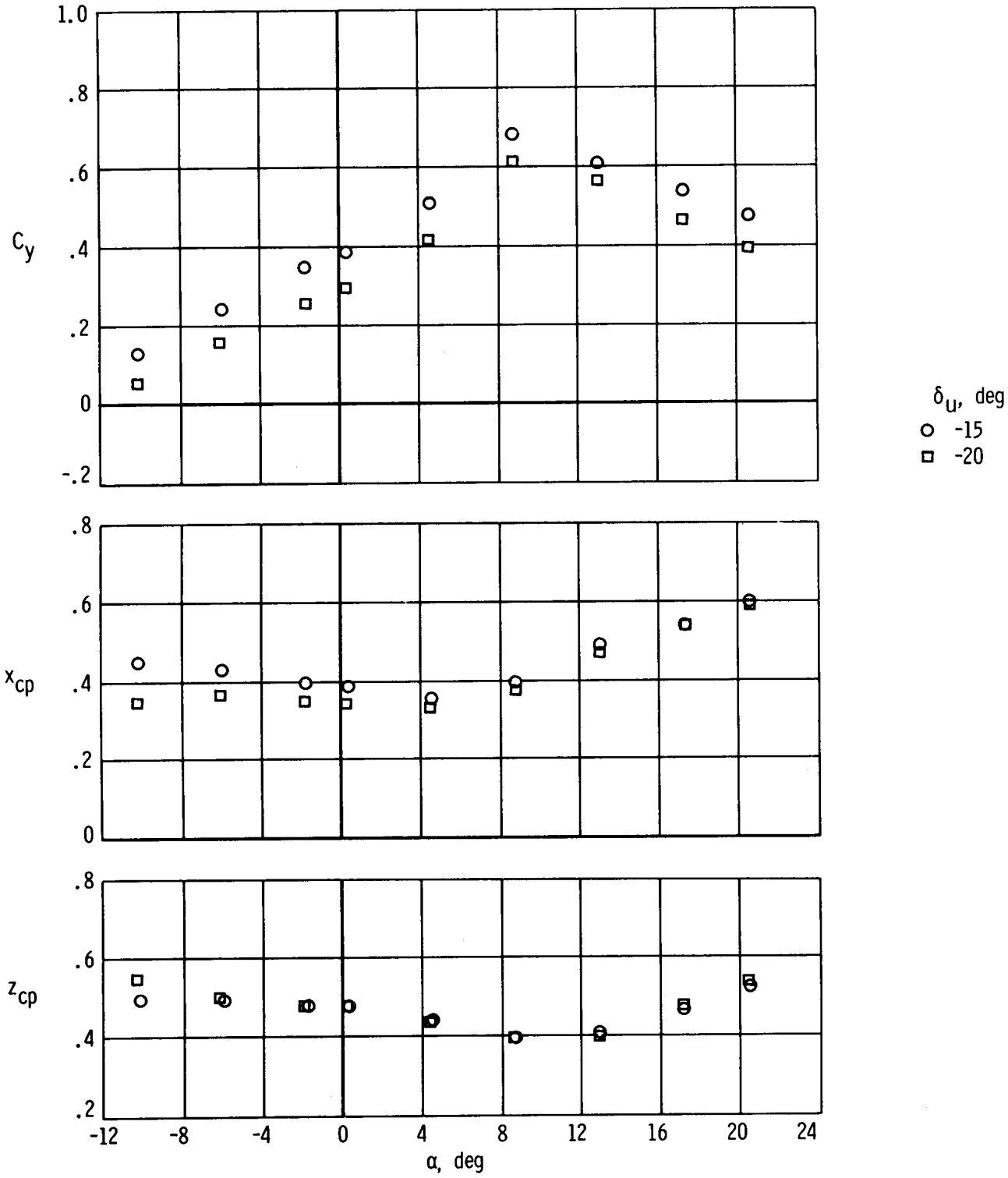

(b) M = 0.70.

Figure 6. Continued.

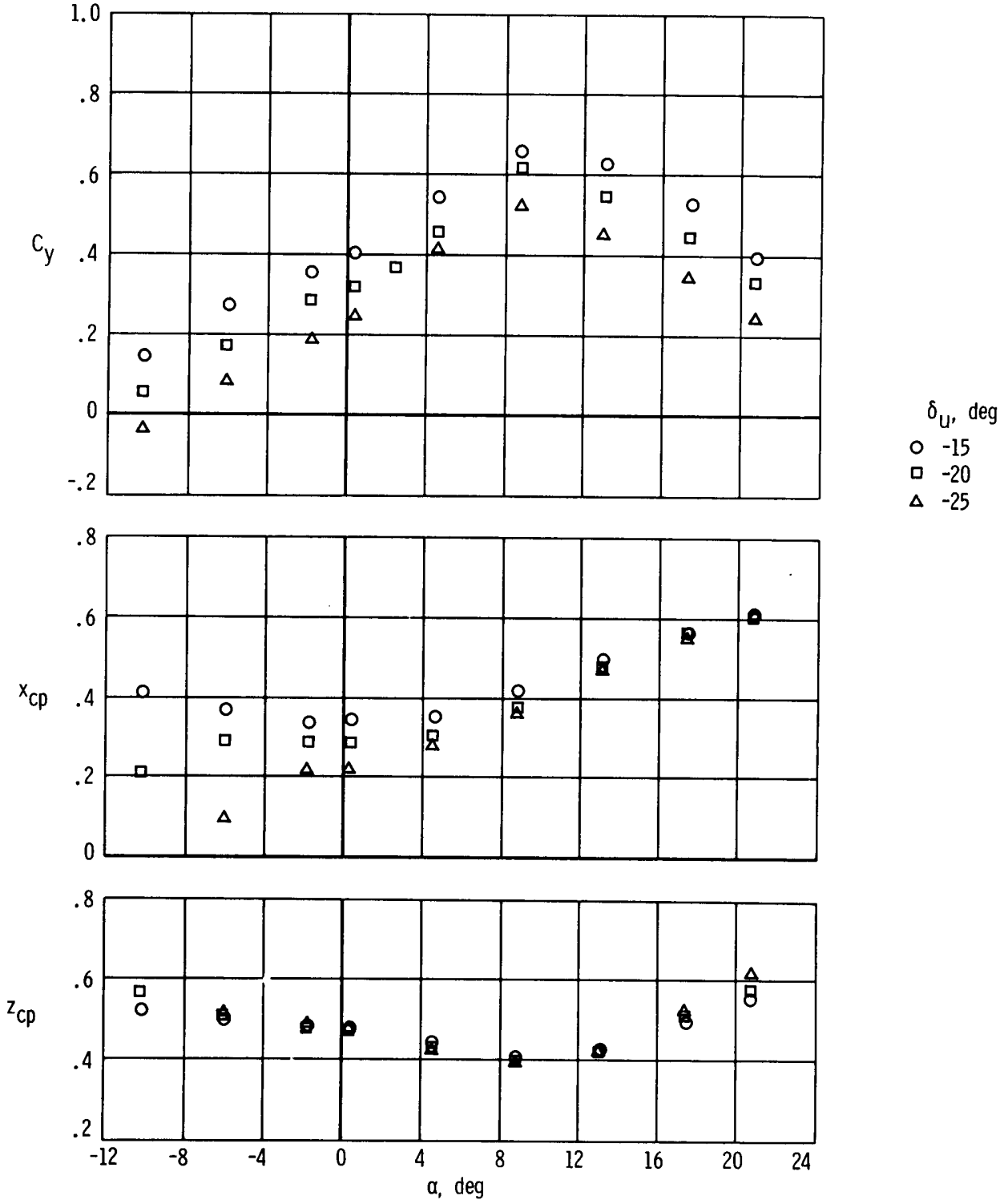

(c) M = 0.80.

Figure 6. Continued.

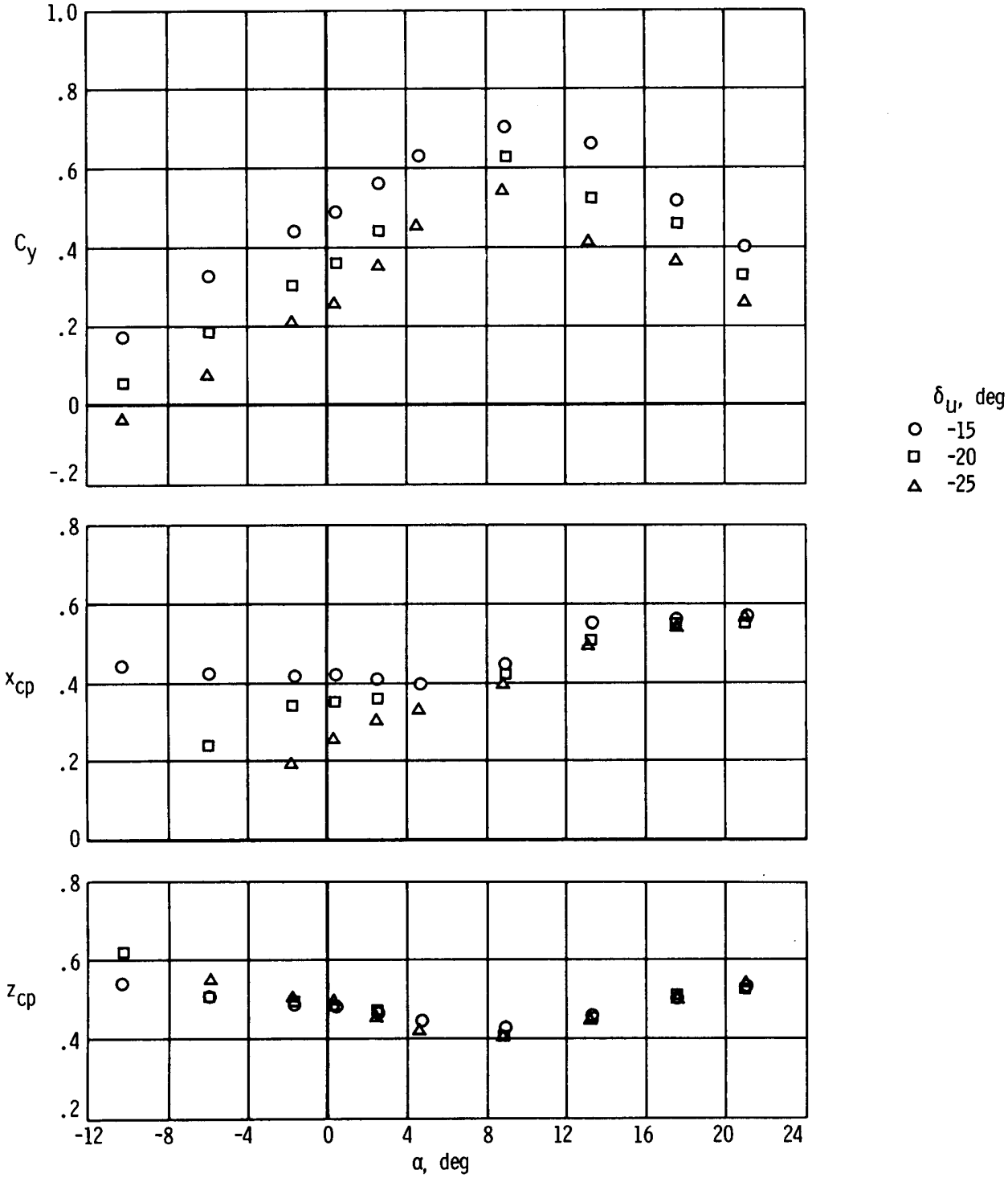

(d) M = 0.90.

Figure 6. Continued.

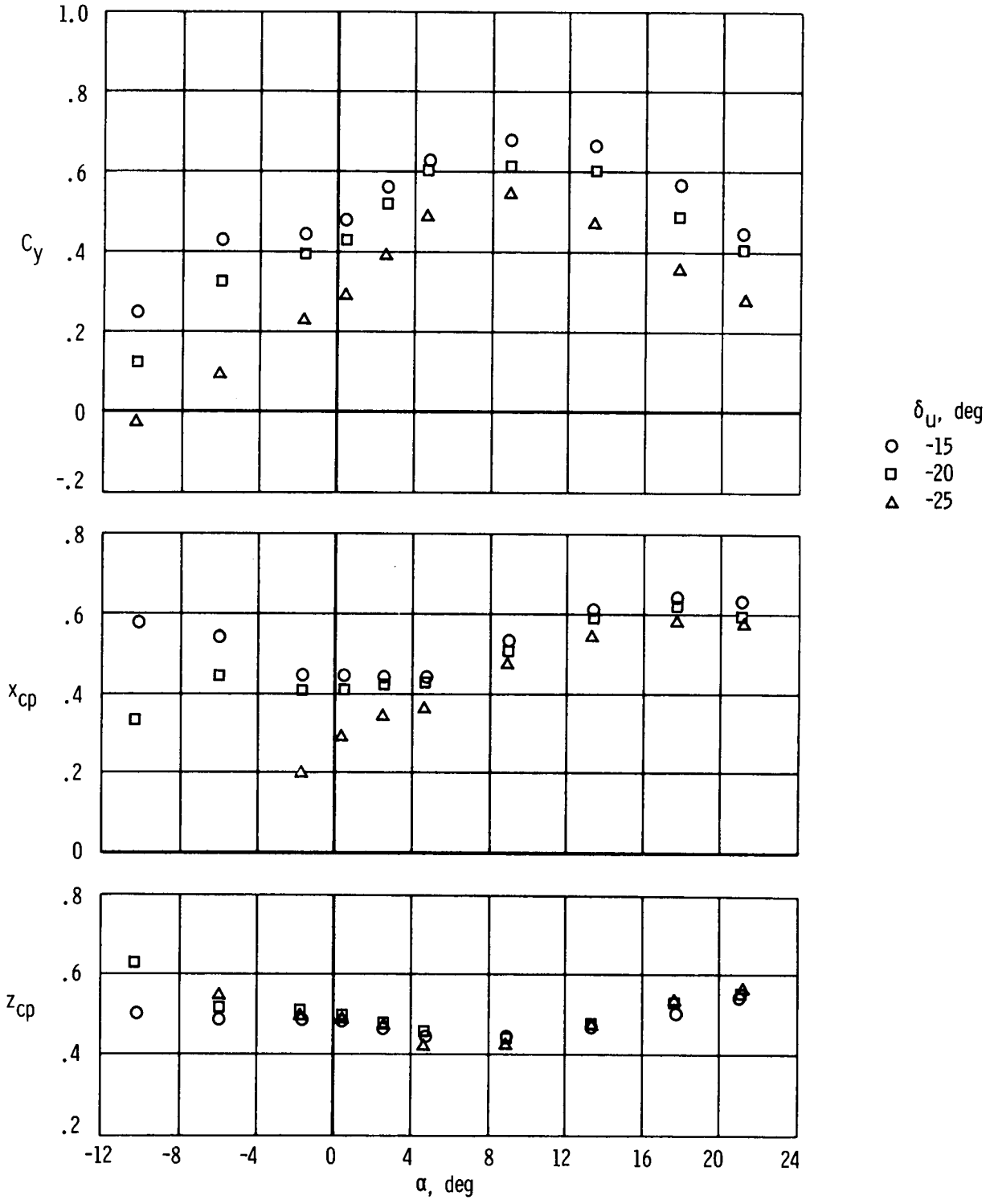

(e) M = 0.95.

Figure 6. Continued.

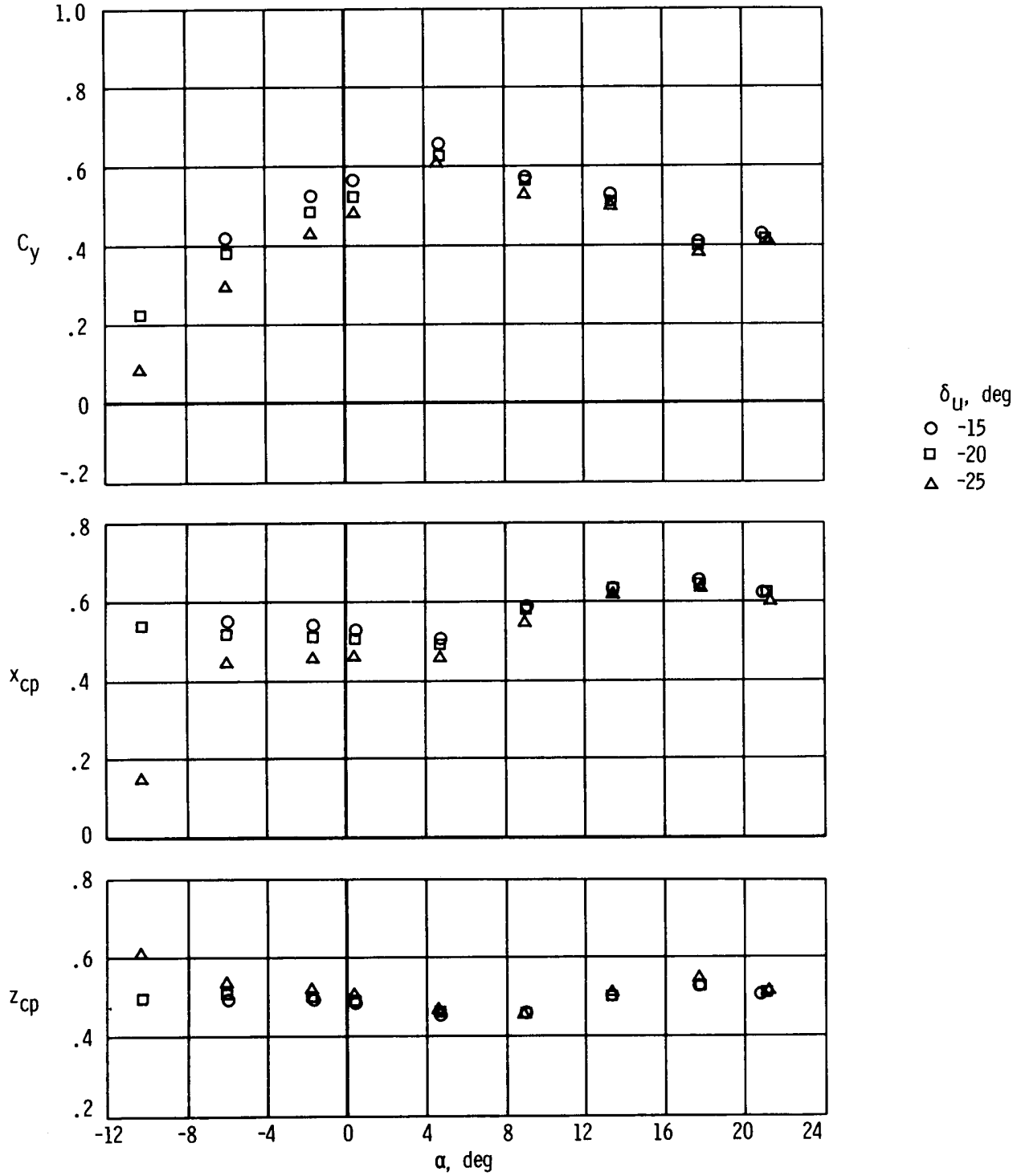

(f) M = 1.10.

Figure 6. Continued.

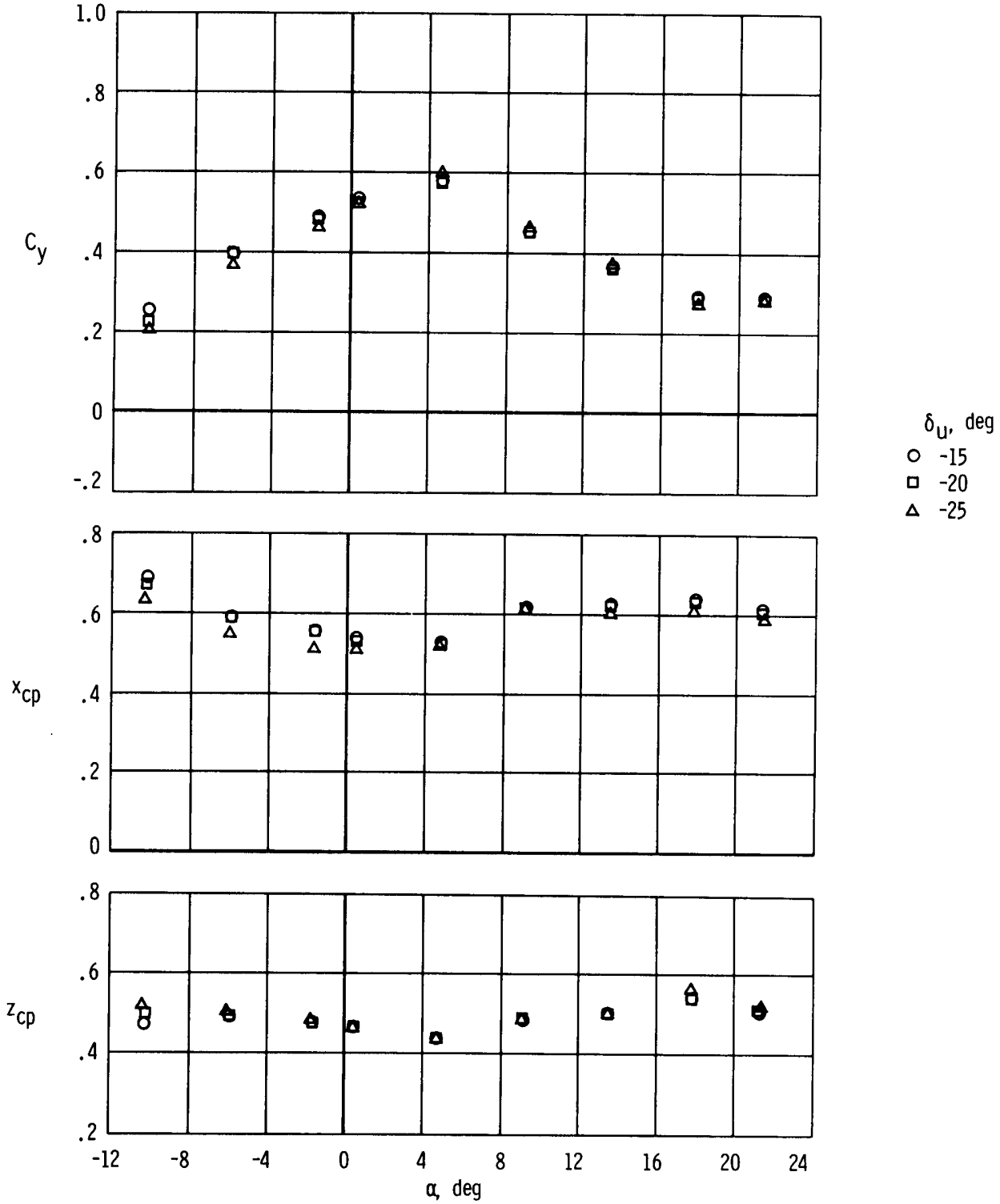

(g) M = 1.30.

Figure 6. Concluded.

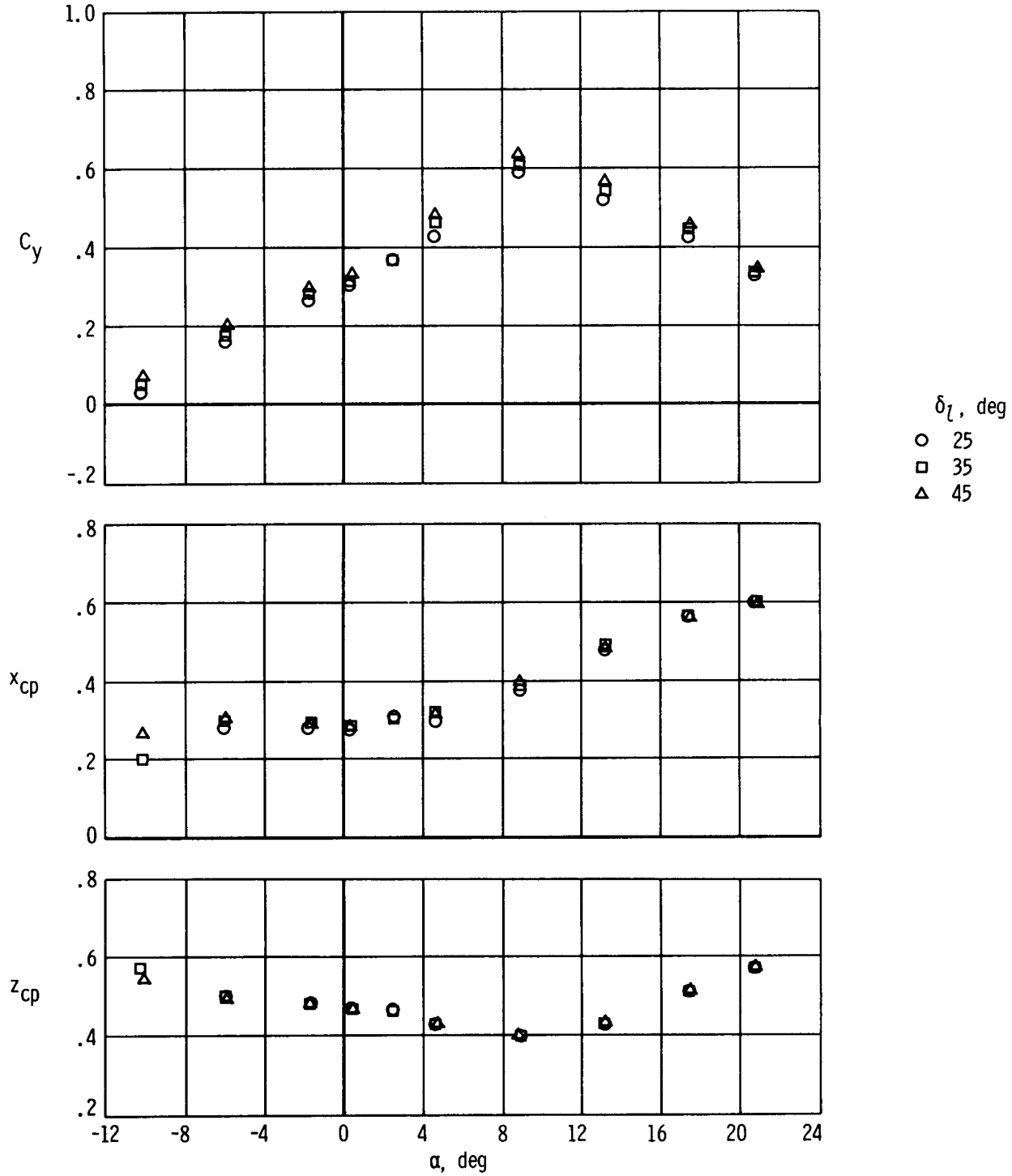

(a) M = 0.80.

Figure 7. Variation of the left-outboard-fin normal-force coefficient and center of pressure with angle of attack and lower-flap position. $\beta = 0°$; $\delta_r = 0°$; $\delta_u = -20°$.

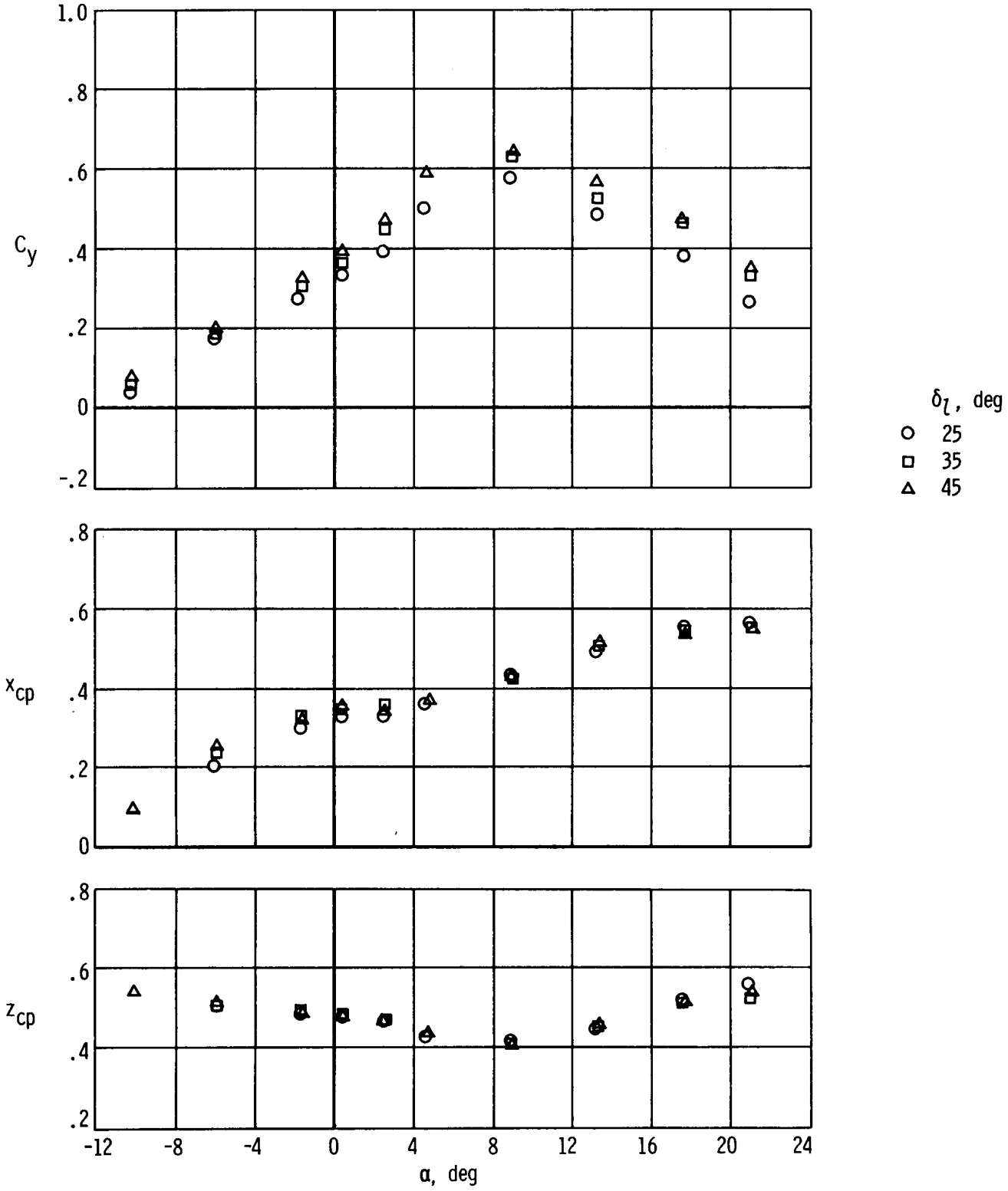

(b) M = 0.90.

Figure 7. Continued.

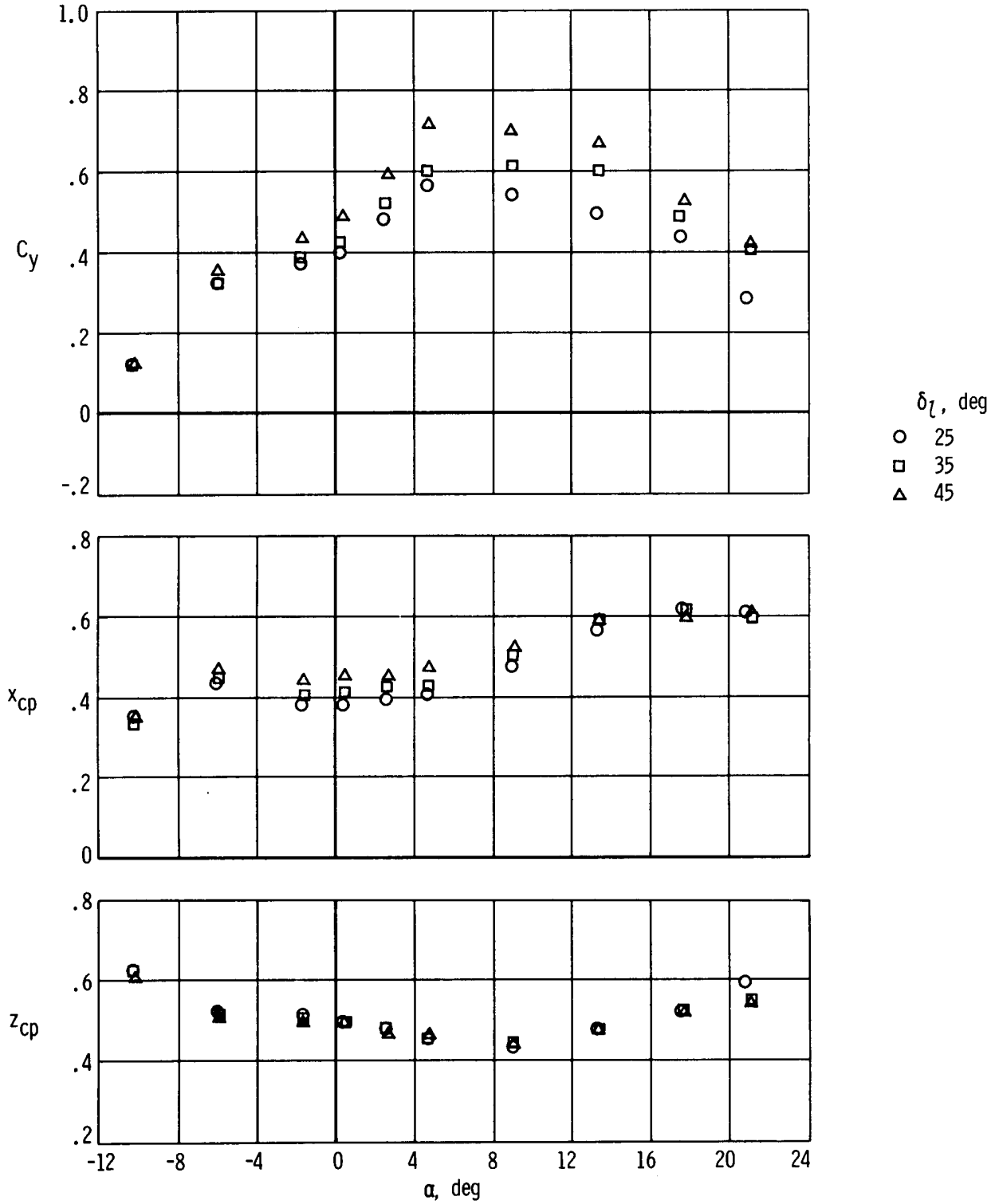

(c) M = 0.95.

Figure 7. Continued.

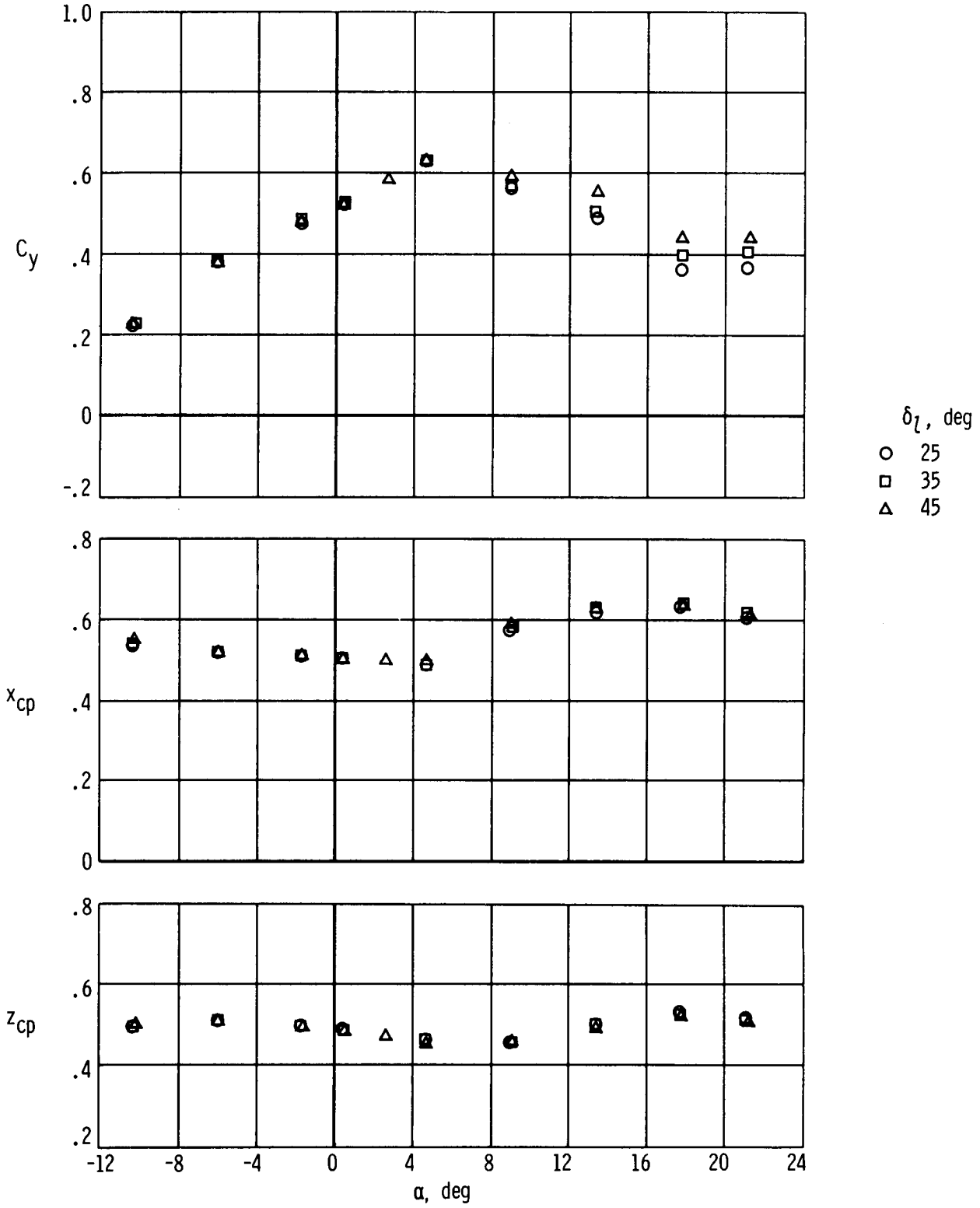

(d) M = 1.10.

Figure 7. Continued.

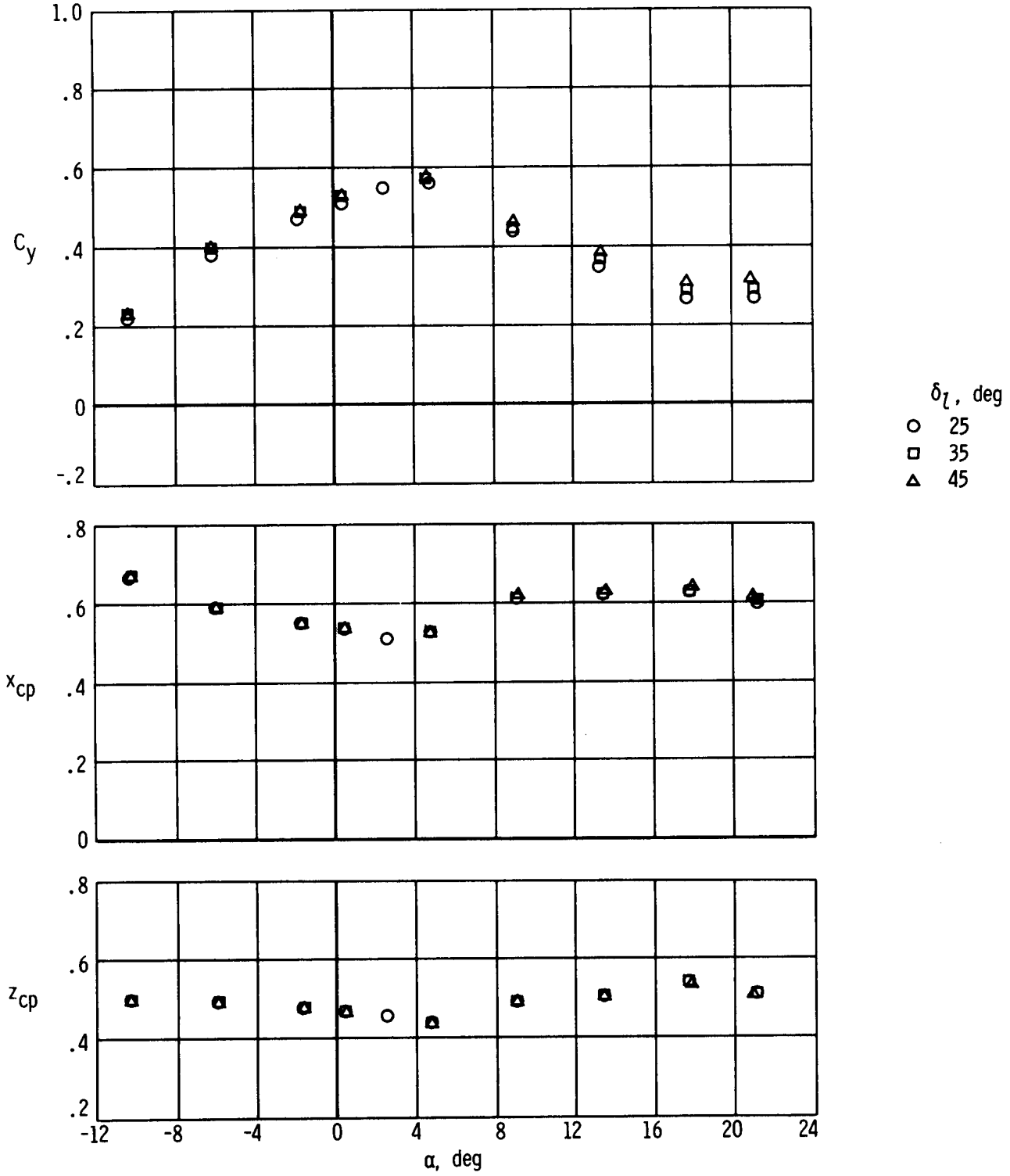

(e) M = 1.30.

Figure 7. Concluded.

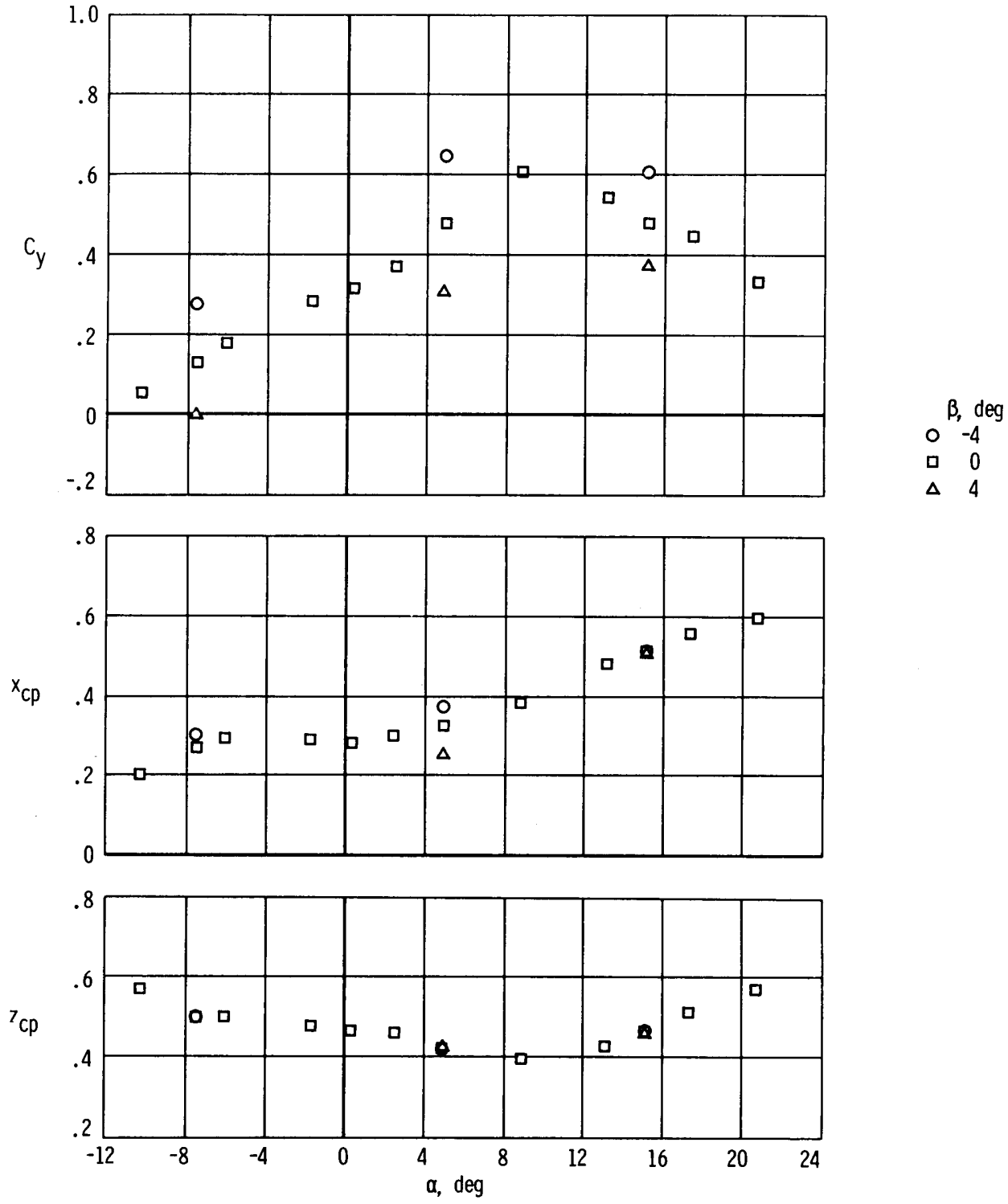

(a) M = 0.80.

Figure 8. Variation of the left-outboard-fin normal-force coefficient and center of pressure with angle of attack and angle of sideslip. $\delta_r = 0°$; $\delta_u = -20°$; $\delta_l = 35°$.

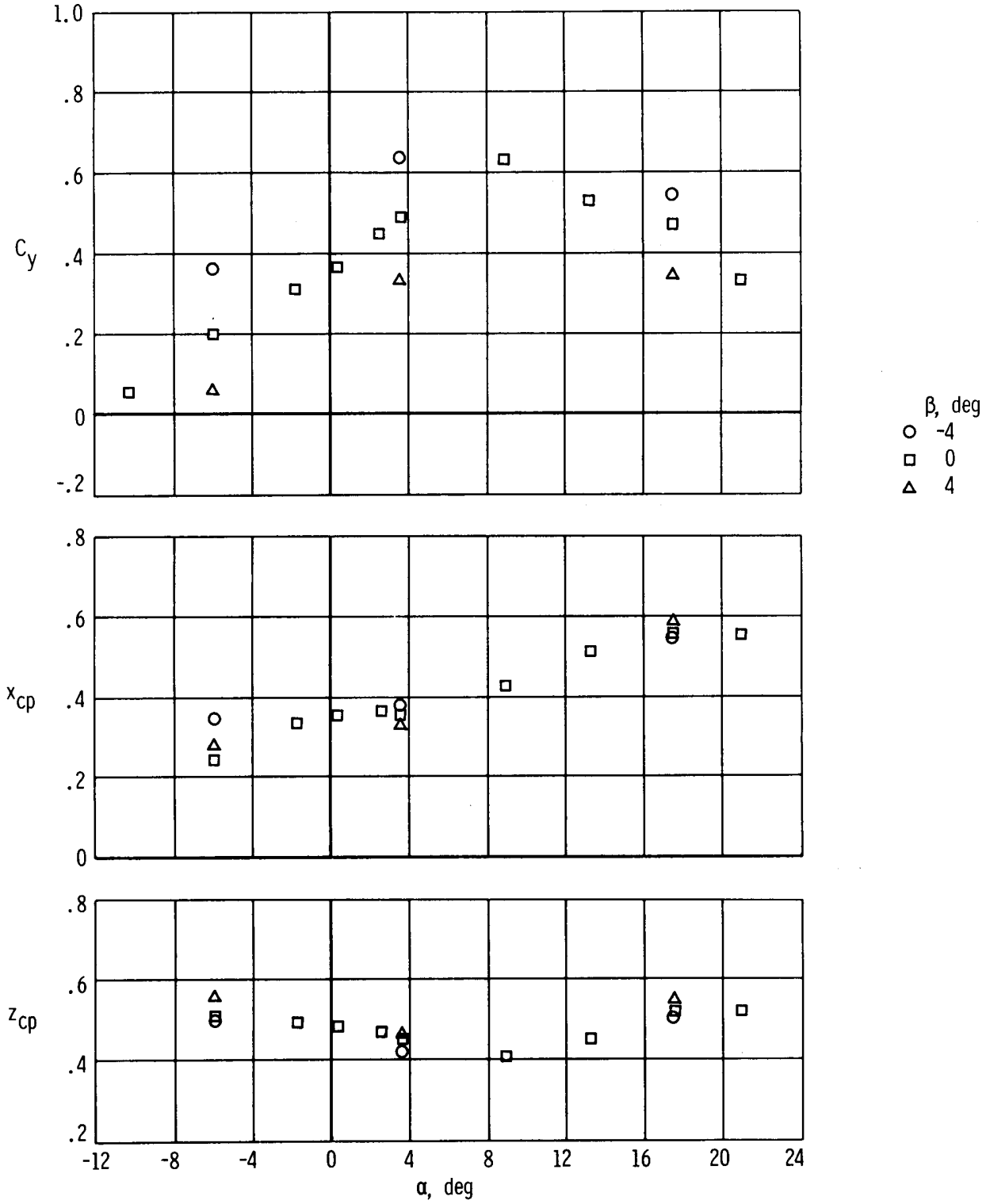

(b) M = 0.90.

Figure 8. Continued.

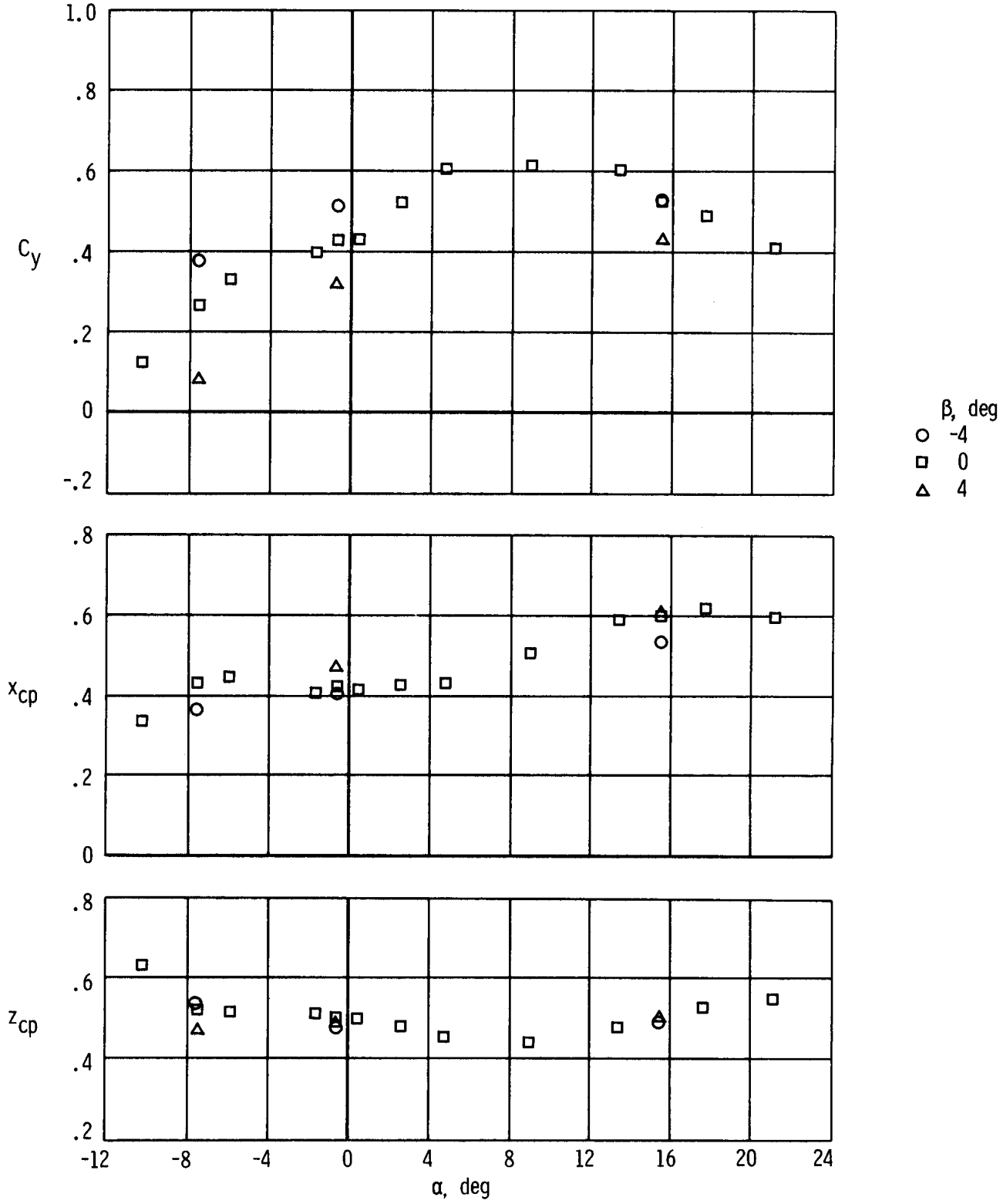

(c) M = 0.95.

Figure 8. Continued.

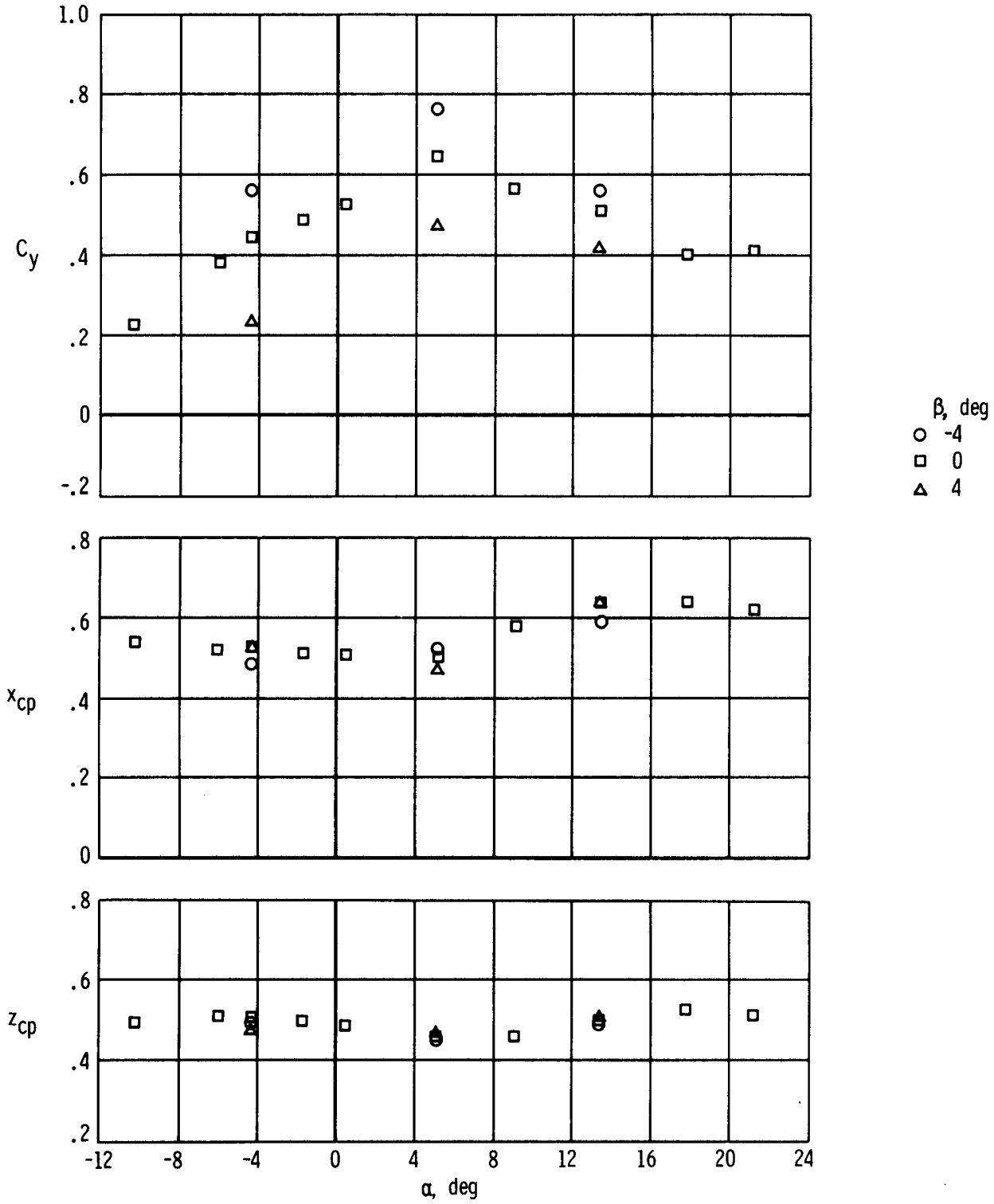

(d) M = 1.10.

Figure 8. Continued.

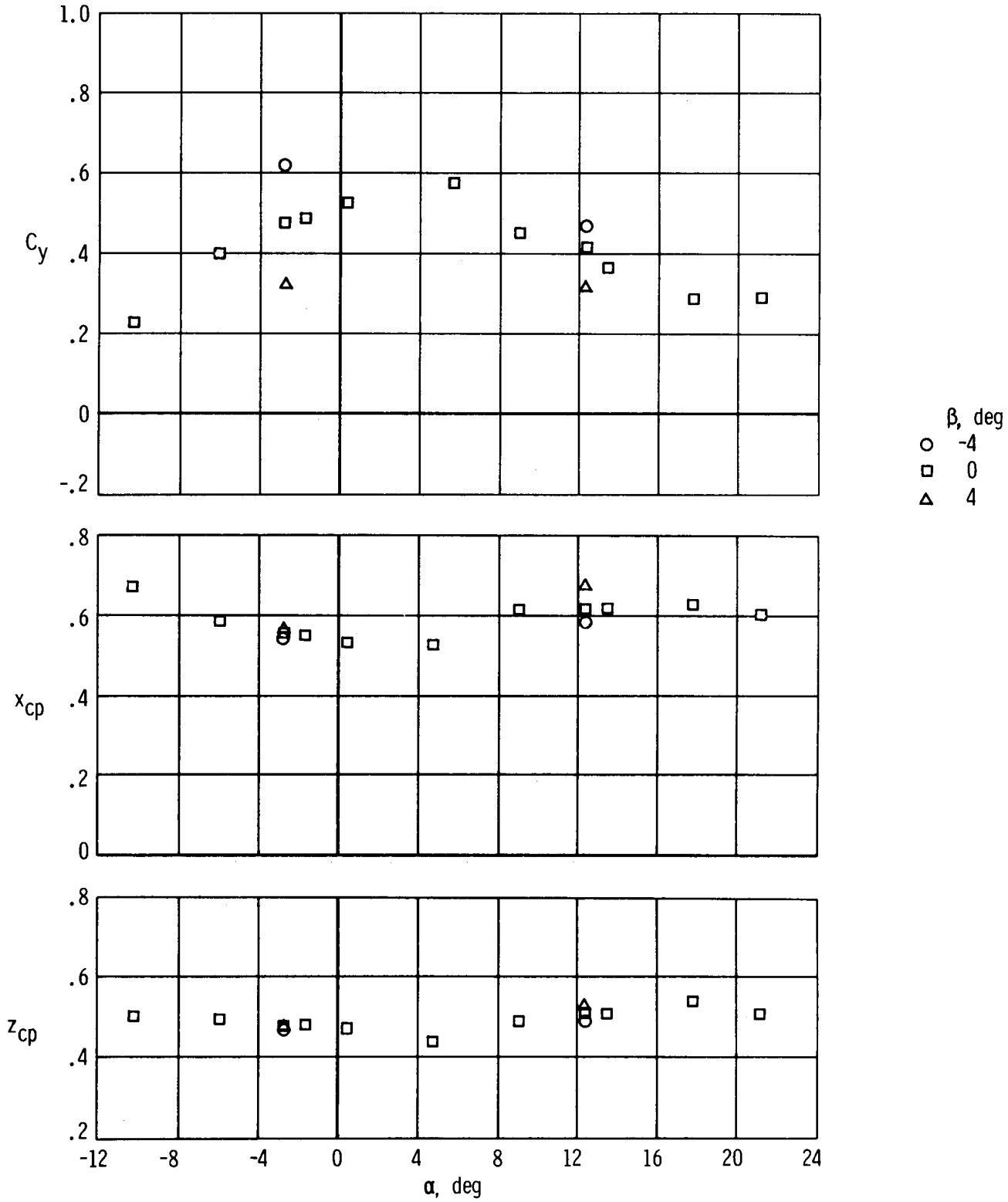

(e) M = 1.30.

Figure 8. Concluded.

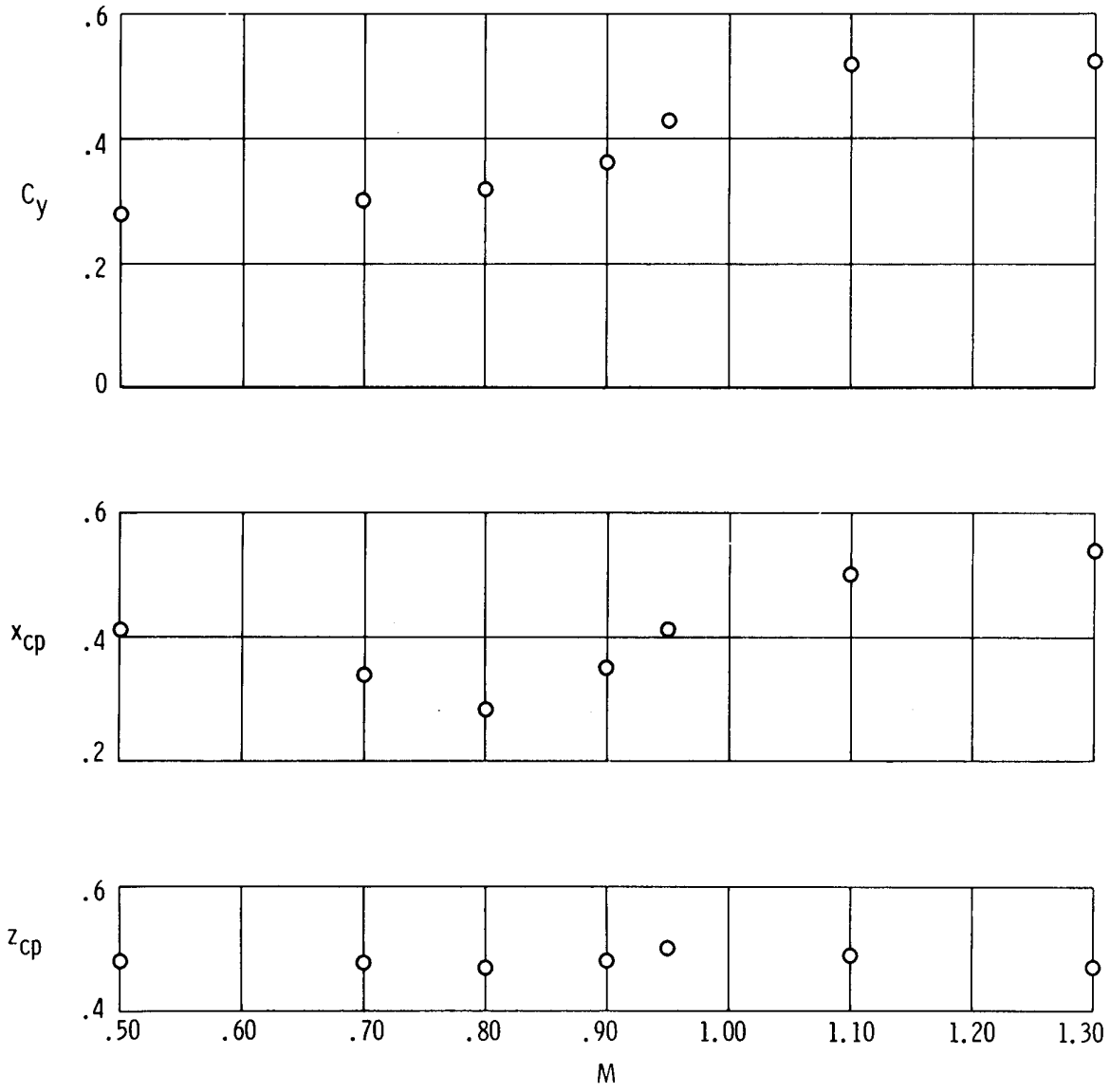

Figure 9. Variation of the left-outboard-fin normal-force coefficient and center of pressure with Mach number. $\alpha = 0°$; $\beta = 0°$; $\delta_u = -20°$; $\delta_l = 35°$; $\delta_r = 0°$.

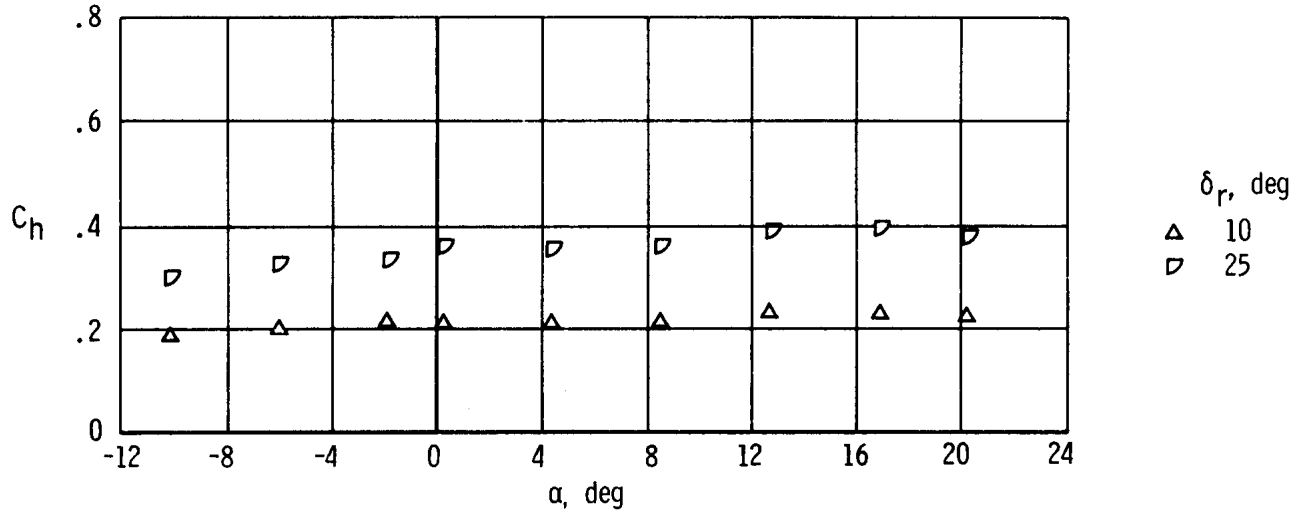

(a) M = 0.50.

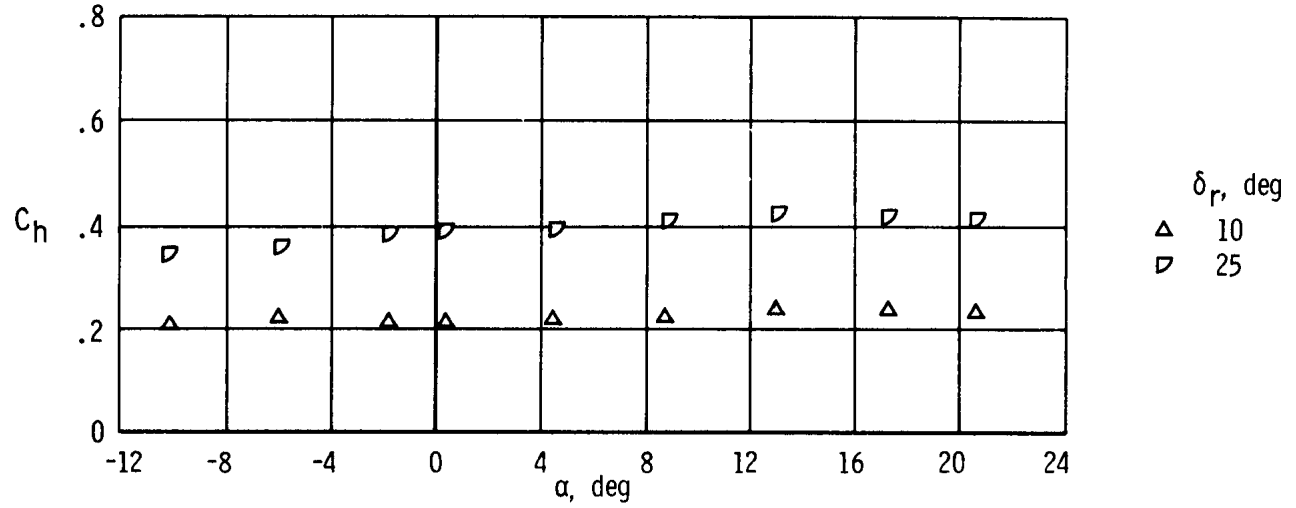

(b) M = 0.70.

Figure 10. Variation of the left-rudder hinge-moment coefficient with angle of attack and rudder position. $\beta = 0°$; $\delta_u = -20°$, $\delta_l = 35°$.

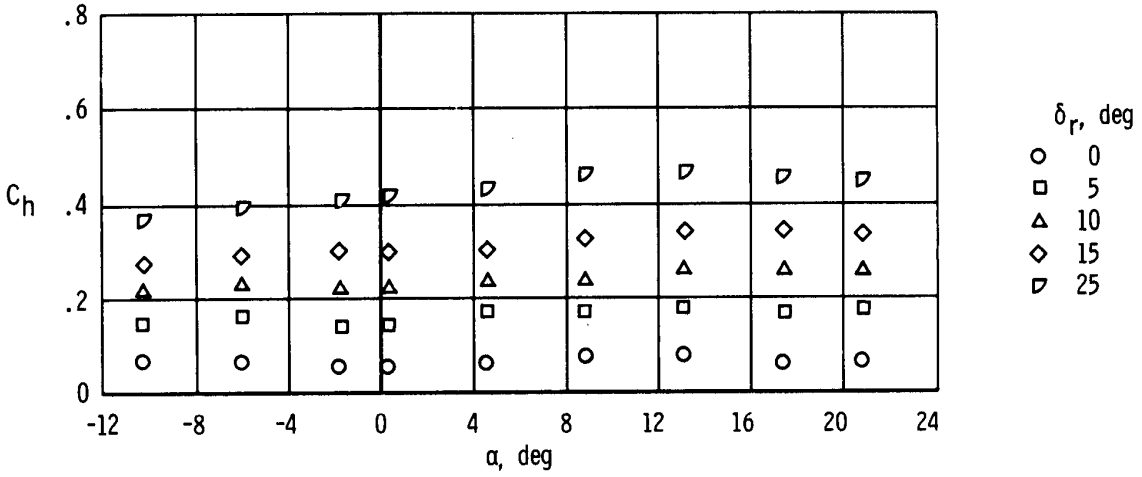

(c) M = 0.80.

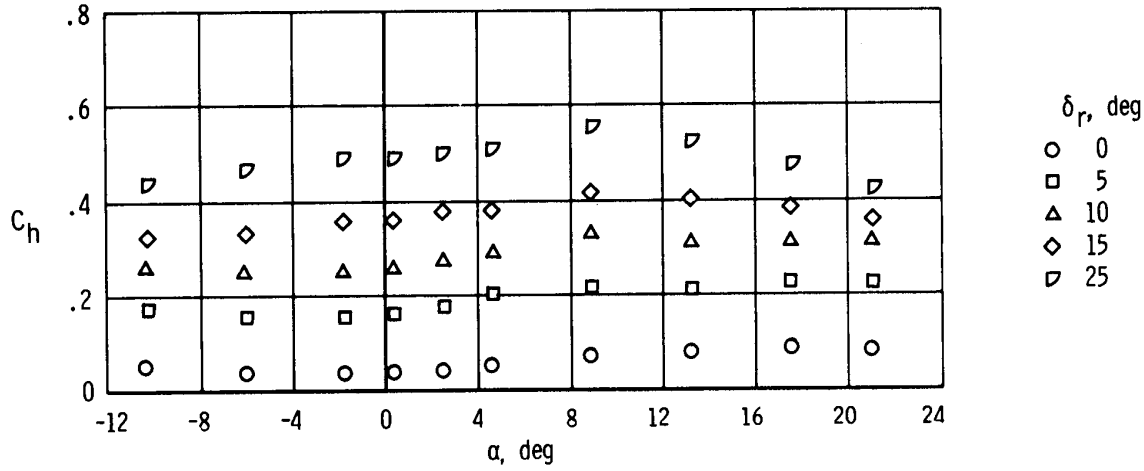

(d) M = 0.90.

Figure 10. Continued.

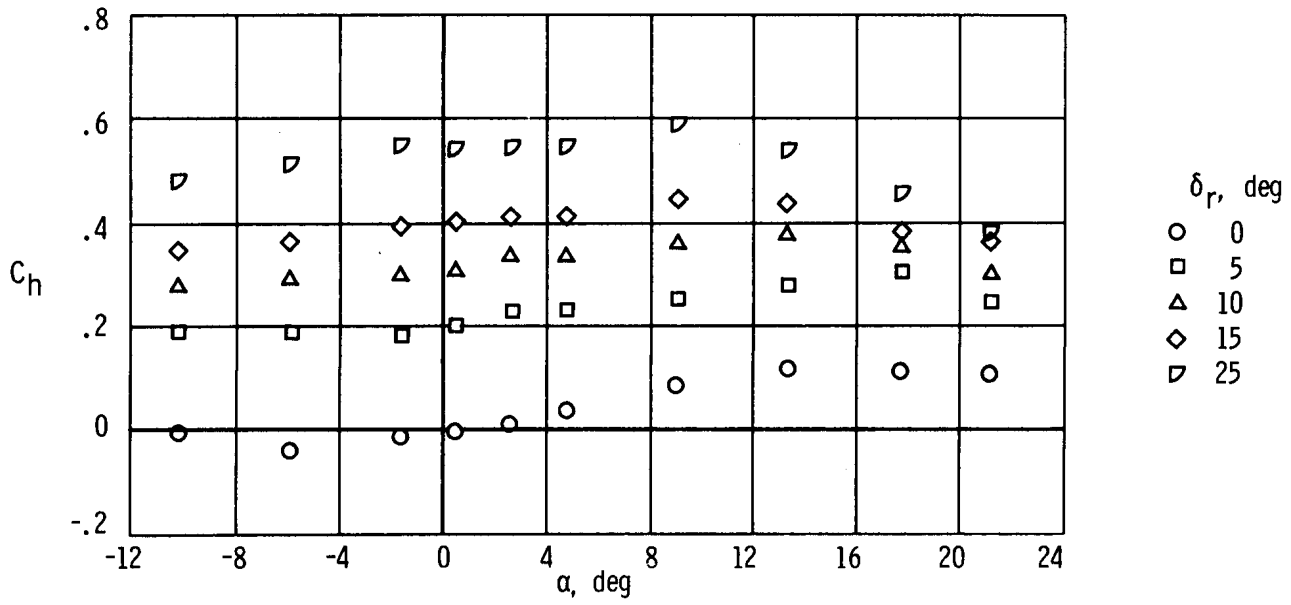

(e) M = 0.95.

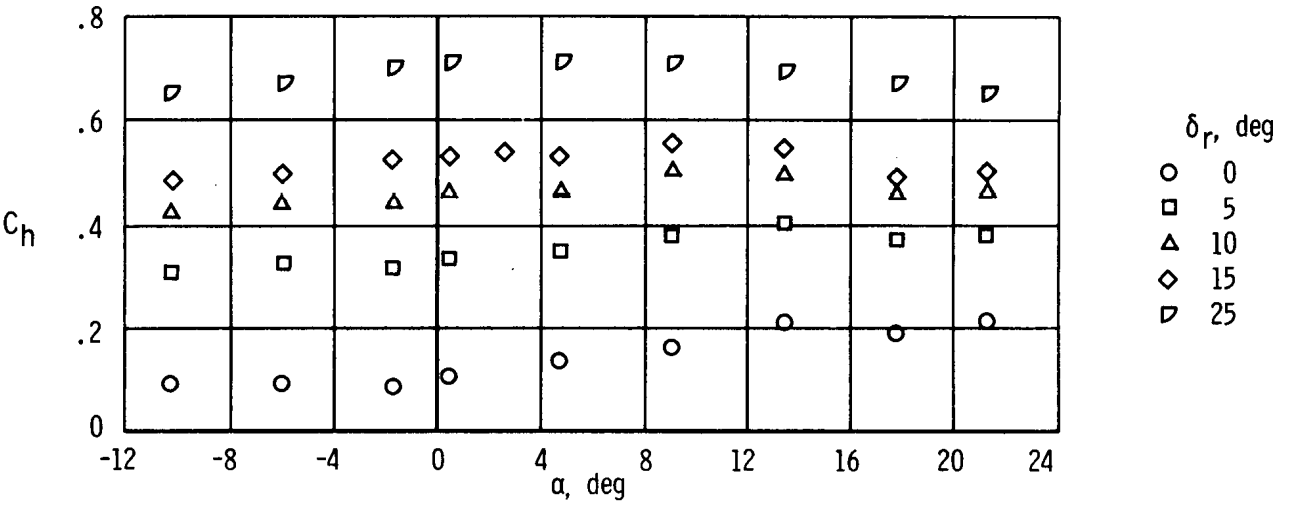

(f) M = 1.10.

Figure 10. Continued.

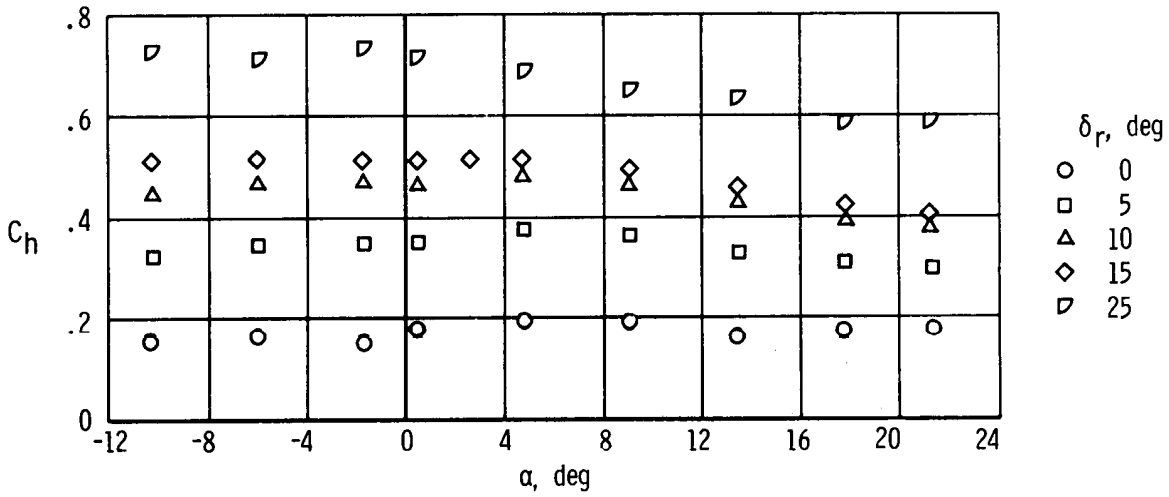

(g) M = 1.30.

Figure 10. Concluded.

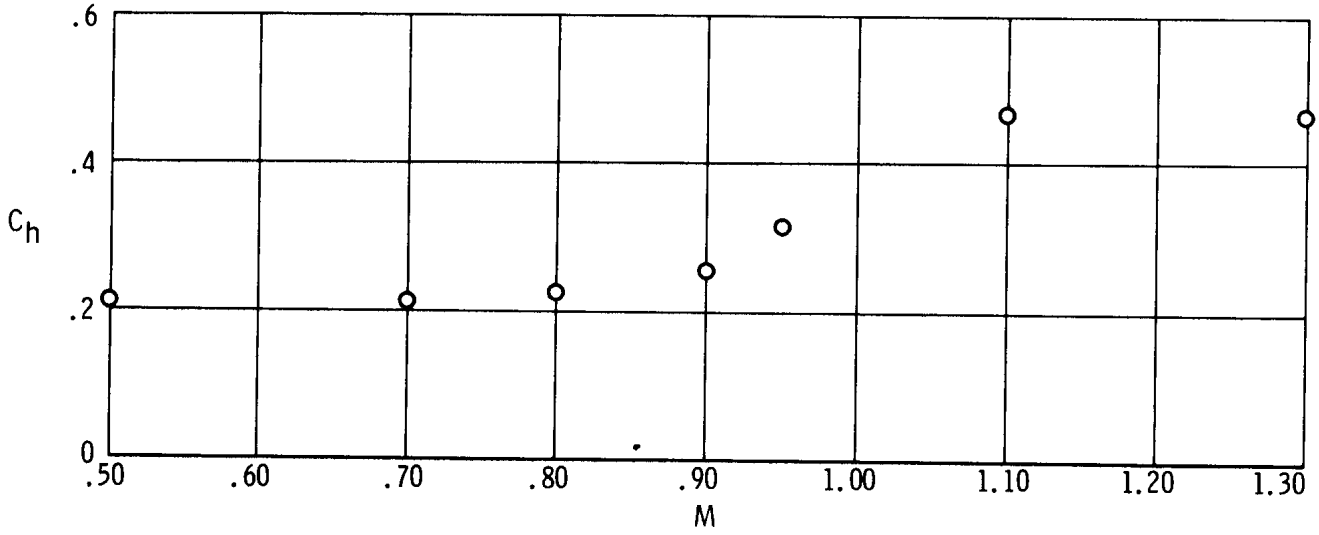

Figure 11. Variation of the left-rudder hinge-moment coefficient with Mach number. $\alpha = 0°$; $\beta = 0°$; $\delta_u = -20°$; $\delta_l = 35°$; $\delta_r = 10°$.

NASA-Langley, 1971 —— 1 H-650